Discovery of the 4-aminopiperidine-based compound EM127 for the site-specific covalent inhibition of SMYD3

Marco Daniele Parenti [a,1], Marina Naldi [c,d,1], Elisabetta Manoni [a], Edoardo Fabini [c], Daniela Cederfelt [e], Vladimir O. Talibov [e,g], Valeria Gressani [h], Ummu Guven [h], Valentina Grossi [i], Candida Fasano [i], Paola Sanese [i], Katia De Marco [i], Alexander A. Shtil [k,l], Alexander V. Kurkin [k], Andrea Altieri [k,m], U. Helena Danielson [e,f], Giuseppina Caretti [h], Cristiano Simone [i,j], Greta Varchi [a], Manuela Bartolini [c,**], Alberto Del Rio [a,b,*]

[a] Institute of Organic Synthesis and Photoreactivity - National Research Council, 40129, Bologna, Italy
[b] Innovamol Consulting Srl, Via San Faustino 167, 41126, Modena, Italy
[c] Department of Pharmacy and Biotechnology, Alma Mater Studiorum University of Bologna, Bologna, Italy
[d] Centre for Applied Biomedical Research, Alma Mater Studiorum University of Bologna, Bologna, Italy
[e] Department of Chemistry – BMC, Uppsala University, 751 23, Uppsala, Sweden
[f] Science for Life Laboratory, Uppsala University, Uppsala, Sweden
[g] BioMAX beam line, MAX IV Laboratory, 22484, Lund, Sweden
[h] Department of Biosciences, University of Milan, 20133, Milan, Italy
[i] Medical Genetics National Institute for Gastroenterology, IRCCS 'S. de Bellis' Research Hospital, Castellana Grotte, Italy
[j] Medical Genetics, Department of Biomedical Sciences and Human Oncology (DIMO), University of Bari Aldo Moro, Bari, 70124, Italy
[k] Department of Chemistry, Lomonosov Moscow State University, Moscow, 119991, Russia
[l] Blokhin National Medical Research Center of Oncology, Moscow, 115478, Russia
[m] EDASA Scientific Srls, 66050, San Salvo (CH), Italy

ARTICLE INFO

ABSTRACT

Recent findings support the hypothesis that inhibition of SMYD3 methyltransferase may be a therapeutic avenue for some of the deadliest cancer types. Herein, active site-selective covalent SMYD3 inhibitors were designed by introducing an appropriate reactive cysteine trap into reversible first-generation SMYD3 inhibitors. The 4-amino-piperidine derivative EM127 (**11C**) bearing a 2-chloroethanoyl group as reactive warhead showed selectivity for Cys186, located in the substrate/histone binding pocket. Selectivity towards Cys186 was retained even at high inhibitor/enzyme ratio, as shown by mass spectrometry. The mode of interaction with the SMYD3 substrate/histone binding pocket was revealed by crystallographic studies. In enzymatic assays, **11C** showed a stronger SMYD3 inhibitory effect compared to the reference inhibitor EPZ031686. Remarkably, **11C** attenuated the proliferation of MDA-MB-231 breast cancer cell line at the same low micromolar range of concentrations that reduced SMYD3 mediated ERK signaling in HCT116 colorectal cancer and MDA-MB-231 breast cancer cells. Furthermore, **11C** (5 μM) strongly decreased the steady-state mRNA levels of genes important for tumor biology such as cyclin dependent kinase 2, c-MET, N-cadherin and fibronectin 1, all known to be regulated, at least in part, by SMYD3. Thus, **11C** is as a first example of second generation SMYD3 inhibitors; this agent represents a covalent and a site specific SMYD3 binder capable of potent and prolonged attenuation of methyltransferase activity.

---

* Corresponding author. Institute of Organic Synthesis and Photoreactivity - National Research Council, 40129, Bologna, Italy.
** Corresponding author.
 E-mail addresses: manuela.bartolini3@unibo.it (M. Bartolini), alberto.delrio@gmail.com (A. Del Rio).
[1] These authors contributed equally to this work.

1. Introduction

Since epigenetic modifications are essential for several cellular mechanisms, epigenetic dysregulation has been implicated in human diseases including cancer [1]. SMYD3 is a methyltransferase (MTase) catalyzing the methylation of specific lysine residues and it is involved in the regulation of gene expression and cell proliferation [2] including histones H3 (Histone H3 Lysine 4, H3K4) and H4 (Histone H4 Lysine 5, H4K5) [3,4], VEGFR1 receptor [5], AKT1 [6], HER2 [7] and MAP3K2 protein [8]. SMYD3 has recently attracted interest of the academic and pharmaceutical sectors as a molecular target for cancer therapy. Consolidated evidence has shown that SMYD3 is overexpressed in several tumors including some of the deadliest ones [9,10] such as breast [11–13], colorectal [14,15], prostate [16,17] and pancreatic cancer, other than gastric and lung cancers, and hepatocellular carcinoma. SMYD3 overexpression has also been correlated with poor prognosis in non-small cell lung cancer [18] and hepatocellular carcinoma [19], and its inhibition has been shown to reduce tumor growth in animal models [20]. Furthermore, preliminary studies have shown that SMYD3 knockout mice have no visible phenotypes [8,21], indicating that this molecular target is dispensable under physiological conditions and that its pharmacological blockade may be well tolerated [8].

Druggability of this target has been demonstrated by our group reporting the first SMYD3 inhibitor BCI-121 (Fig. 1) [14]. Eventually, a number of novel and more potent SMYD3 inhibitors have been identified largely through high throughput screening campaigns [22–24].

Epizyme has developed some of the most potent inhibitors including nanomolar compounds featuring an oxindole and sulfone (EPZ031686 and EPZ030456) functional groups [25] and, more recently, an iso-xazole scaffold and a sulfonamide group (EPZ028862) [24]. The latter fragments are also included in potent GSK derivatives (GSK-49) [24] (Fig. 1). Finally, it is worth mentioning that in 2021 a benzodiazepine-based SMYD3 inhibitor, BAY-6035, was identified and it is currently commercially available [26].

Notwithstanding the involvement of SMYD3 in tumorigenesis, the development of SMYD3 inhibitors was restrained by controversial results [27–29] regarding the role of SMYD3 in tumor cell proliferation. Indeed, SMYD3 silencing did not impair the autonomous proliferation in a large number of cell lines [27]. However, new evidence helped decipher the complexity of the cellular network and mechanisms by which SMYD3 helps supporting tumor growth, for instance by acting as a modulator of transcriptional response and by orchestrating multiple oncogenic traits and, ultimately, promoting transcriptional reprogramming and malignant transformation [20,30]. Importantly, SMYD3 induces the formation of error-free homologous recombination (HR) complexes for DNA restoration by interacting with ATM, CHK2 and BRCA2, thereby propagating the signal cascade and allowing RAD51 loading on DNA lesions [31]. Hence, simultaneous targeting of SMYD3 and PARP leads to synthetic lethality in HR proficient cancer cells [31]. This opens new therapeutic avenues, foreseeing the co-administration of potent and selective SMYD3 inhibitors (SMYD3is) and PARP inhibitors (PARPis) in a poly-pharmacological approach which can be extended to
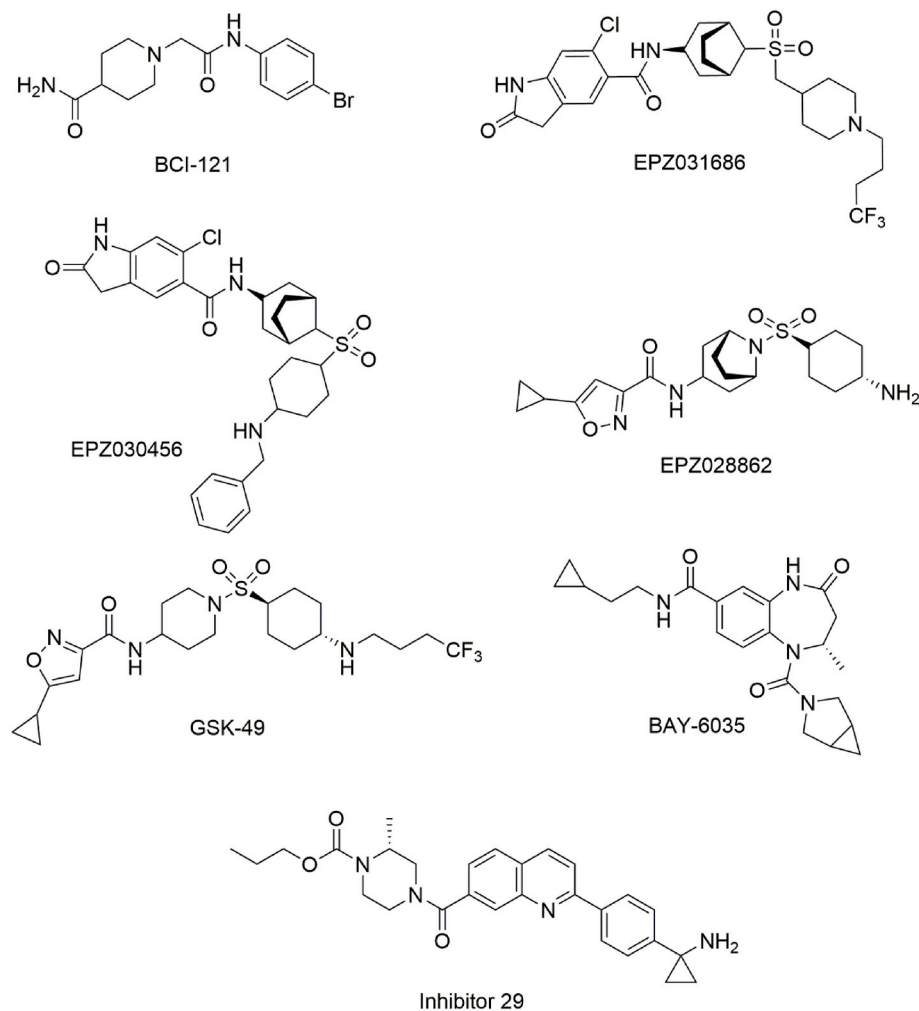

Fig. 1. Chemical structures of BCI-121, EPZ031686, EPZ030456, EPZ028862, GSK-49, BAY-6035 and the irreversible inhibitor 29 developed by Foo and co-workers [22].

cancers that are HR proficient and overexpress SMYD3 [31].

As a part of our on-going interest in the development of selective antitumor compounds and investigations of SMYD3 [14,23,32,33], we envisaged that the development of targeted covalent inhibitors (TCIs) for SMYD3 inhibition would grant a suitable selectivity and long-lasting action [34]. TCIs represent the latest generation of covalent drugs and have already proven to be endowed with suitable safety and efficacy to be approved by FDA for various therapeutic applications including cancer therapy [34]. Selective covalent inhibitors provide a prolonged residence time [35], which has been shown to often drive *in vivo* pharmacodynamic activity and efficacy, rather than affinity. Therefore, compounds capable to covalently modify SMYD3 should be endowed with enhanced efficacy because of a longer residence time as well as long-lasting silencing of MTase activity.

An essential pre-requisite for the rational design of TCIs is the availability of a non-catalytic nucleophilic residue that is poorly conserved across the target protein family. The presence of such a residue has been recently identified by Foo and co-workers during the investigation of the mode of action of a tetrahydroacridine inhibitor, which showed an unconventional irreversible mechanism (see Fig. 1 for structure) [22]. Indeed, in contrast to all other MTases, SMYD3 features a cysteine residue (Cys186) located in the substrate/histone binding pocket, in a solvent-accessible position, approximately 15 Å apart from the cofactor in the middle of the substrate-occupied cavity (see sequence alignment in Fig. S1). Cys186 represents a distinctive feature of SMYD3 that can be exploited for specific targeting, keeping into account that a further key aspect for a successful TCI strategy is the affinity-driven initial interaction prior to covalent binding.

Based on these considerations, we speculated that a strategy to develop TCIs towards SMYD3 could be represented by a suitable modification of an already known and effective SMYD3 reversible inhibitor. Investigation of available scaffolds led to the selection of the oxazole moiety which is a structural feature present in potent and selective SMYD inhibitors [23,24]. Thus, we developed appropriate chemical modifications that introduce a suitable warhead able to act towards the target cysteine in order to create the basis for selective and covalent SMYD3 inhibition. In this study we report the first-in-class rationally designed 4-aminopiperidine-based TCIs as SMYD3 inhibitors. Since covalent binding should be carefully tuned to avoid non-specific binding, a high-resolution mass spectrometry (MS) and surface plasmon resonance (SPR) biosensor techniques were applied to characterize the mode of action at the isolated target to confirm the targeting of Cys186, and to guide the selection of optimal candidates for cell-based investigations on HCT116 colorectal cancer and MDA-MB-231 breast cancer cell lines. Derivatives lacking the cysteine trap functionality were also synthesized and assayed to dissect the affinity from the reactivity and speculate on the importance of a long-lasting inactivation of SMYD3 for anticancer properties.

2. Results and discussion

2.1. De novo design

Taking advantage of the structure of EPZ028862 (Fig. 1), two different scaffolds were designed for the synthesis (Fig. 2). Based on previously reported data, the isoxazole scaffold was selected as the most suitable SMYD3 binding moiety [23,24]; this was connected through an amide bond to a piperidine substituent bearing the reactive Cys186 trap either at the position 4 of the piperidine ring (A, Fig. 3) or directly bound to the piperidine amino group (B, Fig. 3). The piperidine group was specifically selected because docking simulations performed showed a good shape complementarity in the SMYD3 binding site in the proximity of Cys186.

Based on these premises, six compounds were synthesized bearing the molecular scaffolds A or B (Fig. 3). Covalent inhibitors were identified with "C" to discriminate from non-covalent ones.
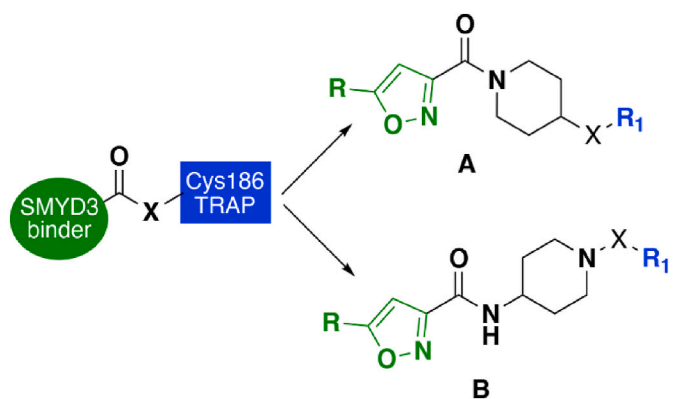

Fig. 2. Chemical representation of scaffolds A and B bearing the fragment of the SMYD3 binding site and a reactive warhead (R$_1$) for covalent binding to Cys186.
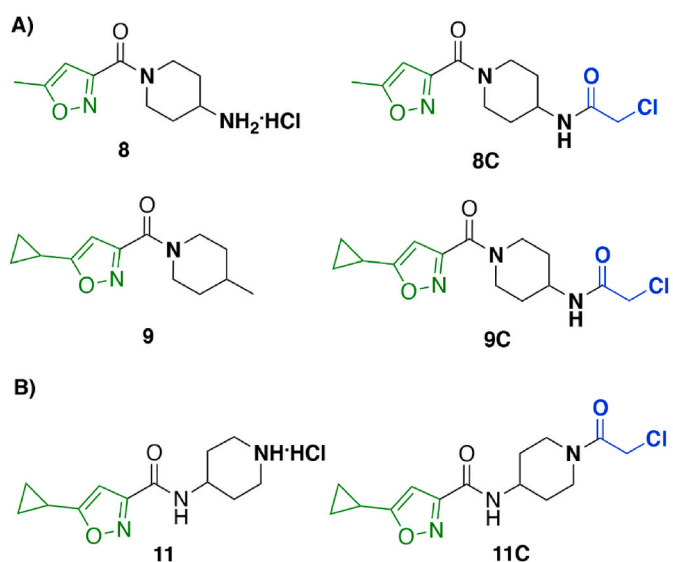

Fig. 3. Chemical structures of newly synthesized SMYD3 non-covalent inhibitors **8**, **9** and **11** and corresponding covalent analogs **8C**, **9C** and **11C** (also known as EM127).

2.2. Chemistry

The synthesis of piperidine-based compounds bearing the reactive moiety at the 4-position of the piperidine scaffold, namely scaffold A, is shown in Scheme 1. The reaction of 1-NH-Boc-4-aminopiperidine (**1**) with 2-chloroacetyl chloride in pyridine/CH$_2$Cl$_2$ mixed solvent afforded compound **2** (90% yield) which, upon deprotection of the amino group under standard conditions, provided the building block **3** in a quantitative yield. Subsequently, the 5-substituted-isoxazole-3-carboxylic acids **4** and **5** reacted with 4-Boc-aminopiperidine to give corresponding derivatives **6** and **7** which were readily deprotected under standard conditions to afford non-covalent inhibitors **8** and **9** in 53% and 96% yields, respectively. Alternatively, compounds **4** and **5** were reacted with **3** under standard EDC coupling conditions to afford covalent inhibitors **8C** and **9C** in 40% and 75% yields, respectively (Scheme 1).

For the synthesis of **11** and **11C** (Scheme 2), the 5-cyclopropylisoxazole-3-carboxylic acid **4** was reacted with 1-Boc-4-aminopiperidine **1** to afford the corresponding amide **10** in 58% yield; deprotection under standard acidic conditions provided the free amine **11** in a quantitative yield. Finally, by reacting **11** with 2-chloroacetyl chloride in the presence of DIPEA, compound **11C**, also designated as EM127, was obtained in 96% yield upon purification.
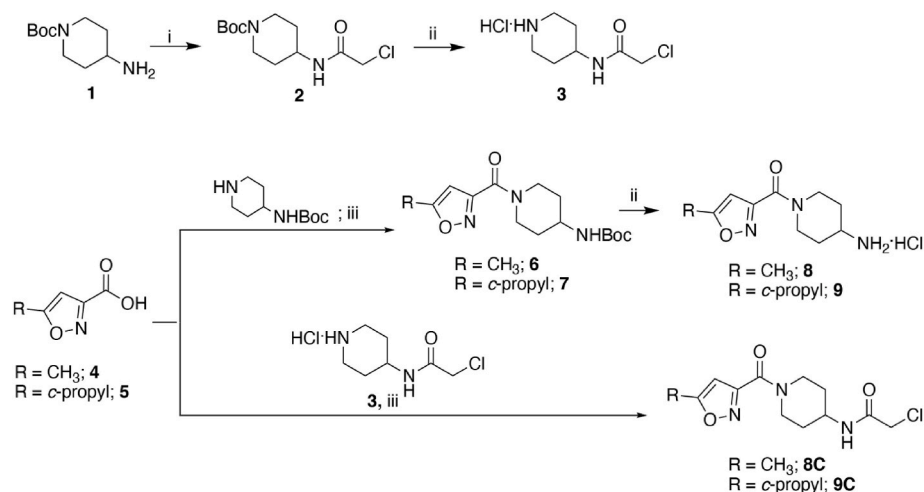
Scheme 1. Synthesis of SMYD3 covalent inhibitors **8C** and **9C** and their non-covalent analogs **8** and **9**.a (i) 2-chloroacetyl chloride, pyridine, CH_2Cl_2, 0 °C to rt; (ii) HCl (2 M), MeOH; (iii) EDC, DIPEA, CH_2Cl_2, rt.
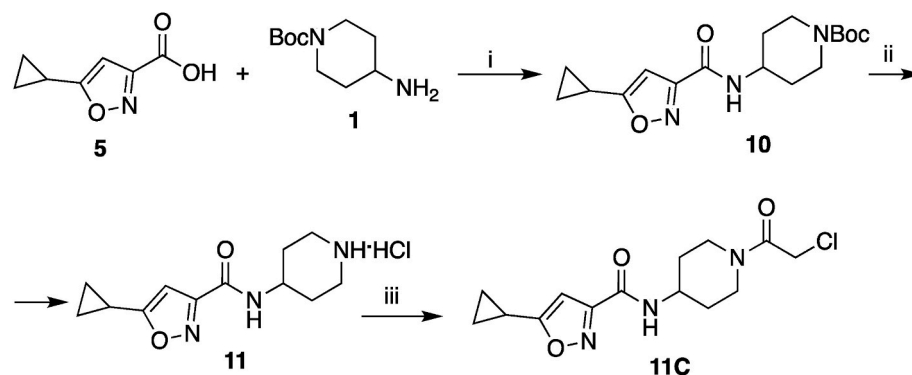
Scheme 2. Synthesis of SMYD3 covalent inhibitor **11C** (EM127) and its non-covalent analog **11**.a (i) EDC, DIPEA, CH_2Cl_2, rt; (ii) HCl (2 M), MeOH; (iii) 2-chloroacetyl chloride, DIPEA, CH_2Cl_2, 0 °C to rt.

2.3. Binding affinity studies by SPR biosensor analysis

Since binding to the target is a prerequisite for a TCI to be effective, we first investigated the interaction between SMYD3 and all derivatives by SPR biosensor technology. Compounds were tested in the presence and absence of saturating concentration of the cofactor S-adenosyl methionine (SAM) in the running buffer to monitor the effect of the cofactor on the binding of the inhibitors. While no interaction with immobilized SMYD3 could be observed for compound **8C** and the corresponding reversible analog **8** under any conditions, the other tested compounds only showed interactions with the enzyme when SAM was present in the running buffer. Under these conditions, the isoxazole amides **11** and **11C** showed a significantly higher affinity to SMYD3 and responses in agreement with control compounds S-adenosyl homocysteine (SAH) and MAP3K2$_{249-274}$, a 26 amino acid peptide which carries the MTase target amino acid Lys260, while **9** and **9C** produced low responses at all tested concentrations (100 and 1.56 μM). For **11** and **11C**–complexes, the steady-state affinity constants (K_D) in the presence of SAM were estimated. Because of relatively short time course of the experiment (within 60 s) no covalent modification of SMYD3 was detected in agreement with the longer time required for the formation of a covalent adduct, as shown by liquid-chromatography mass spectrometry (LC-MS) experiments (see section 4.4). Interactions between **11** or **11C** and SMYD3 were characterized by fast association and dissociation rates, as expected for these small compounds interacting with relatively weak affinities (Fig. 4). The signal responses at steady-state fitted with a 1:1 binding stoichiometry, based on the apparent

surface activity found for control compounds SAH and MAP3K2$_{249-274}$ peptide. Thus, a simple binding isotherm was used to estimate the affinities as K_D values, being 32 $\pm$ 7 μM for **11** and 13 $\pm$ 2 μM for **11C**. Note that, the estimates were obtained *via* an extrapolation since the concentrations that could be used were not high enough to reach saturation.

2.4. Investigation of the mechanism of inhibition by MS

Classical ESI-MS analysis can be used to easily distinguish covalent *vs* non-covalent target-ligand complexes. Indeed, a covalent enzyme-ligand adduct is not cleaved during the desorption/ionization process within an electrospray ion source, while a non-covalent enzyme-ligand complex is. Hence, if formation of a covalent adduct occurs, a new signal at higher *m/z* values is expected to appear in the MS spectrum, as a consequence of enzyme mass increase upon covalent binding formation. This assay is performed on the intact protein without any further processing. Hence, to assess whether the three derivatives bearing the reactive warhead were able to covalently bind SMYD3, an ESI-MS analysis was performed on intact SMYD3 upon incubation with a 10-fold molar excess of either **8C**, **9C** and **11C**. Inspection of mass spectra confirmed that **9C** and **11C** were able to form a covalent adducts, while no stable adduct was detected upon incubation with **8C**. These results are consistent with the inability to detect an interaction between **8C** and SMYD3 using the SPR biosensor assay. Thus, the lack of binding likely prevents a suitable localization of the inhibitor close to Cys186 within the target binding pocket. The derivative **9C** differs from **8C** in the
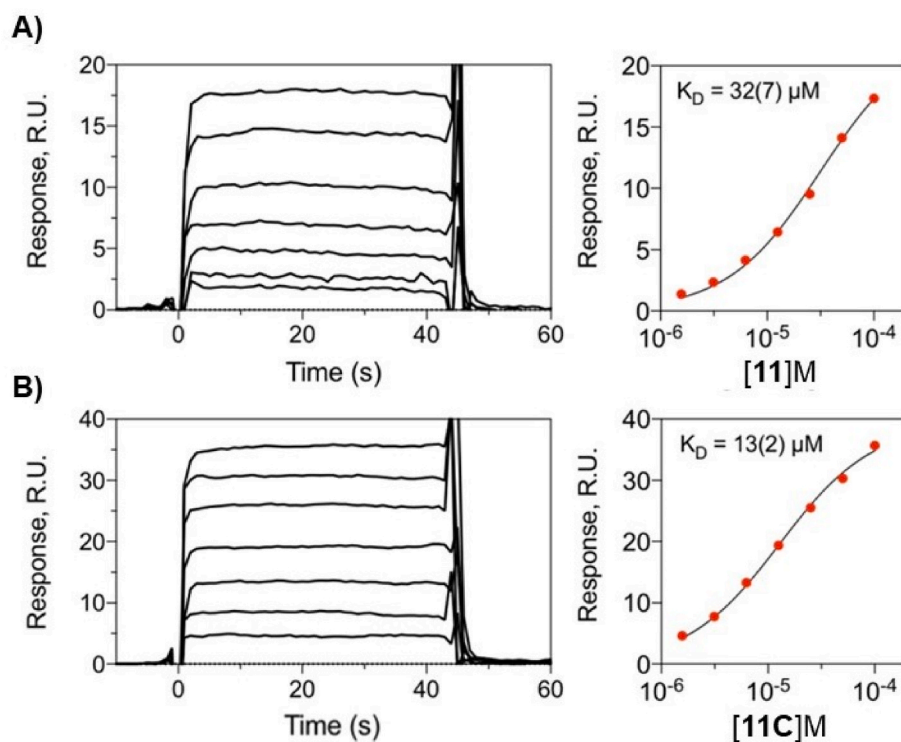
Fig. 4. Representative sensorgrams for the interaction of compounds with immobilized SMYD3 in the presence of SAM in the running buffer. A) Sensorgrams (left) and response at equilibrium fitted to a 1:1 interaction model (right) for **11** interacting with immobilized SMYD3. B) Sensorgrams (left) and response at equilibrium fitted to a 1:1 interaction model (right) for **11C** interacting with immobilized SMYD3. Experiments were carried out in duplicate.

cyclopropyl instead of the methyl substituent on the oxazole group. Hence, the cyclopropyl group seems to be essential for a stable anchorage in the SMYD3 active site, thereby favouring the reaction between the nucleophilic Cys186 and the reactive group of our derivatives.

The specific site of reaction of **9C** and **11C** along the SMYD3 primary structure was also assessed by searching for modified peptides upon protein digestion (see supporting information for experimental details); results showed that both **9C** and **11C** were able to target Cys186, located in the substrate binding site, in a concentration-dependent manner (Fig. 5 and Table S2), being **11C** significantly more effective in forming a covalent adduct, also in agreement with its higher apparent affinity.

Interestingly, **11C** showed a striking selectivity for the target Cys186 residue, even in conditions in which reaction was forced (inhibitor/SMYD3 ratio equals to 10) and 100% of targeted amino acid was covalently modified (Fig. 5). SMYD3-**11C** formation showed to be
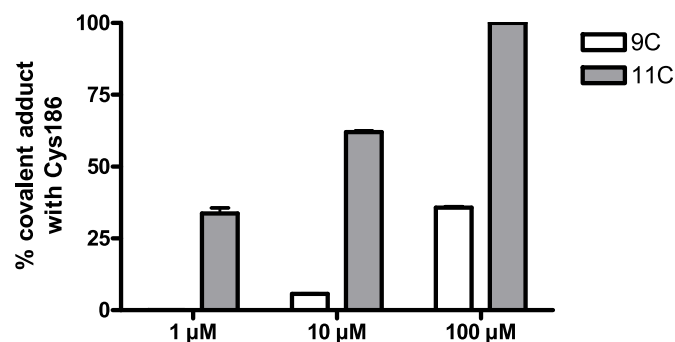
concentration-dependent (Fig. 5 and Table S2) with high yield of reaction. Conversely, despite compound **9C** was endowed with good selectivity when incubated with SMYD3 at equimolar ratio (no covalent adducts with other cysteine residues were detected), selectivity towards Cys186 was lost when a higher inhibitor/enzyme ratio was assayed and modification of Cys238 was observed (% adduct formation = 13.0 $\pm$ 0.7) at **9C**/SMYD3 ratio of 10 (Table S2). Furthermore, the extent of the covalent adduct formed by **9C** with the target Cys186 at equimolar ratio with SMYD3 was very low (5.7%).

As expected for a covalent inhibitor, the formation of the covalent adduct between **11C** and SMYD3 was shown to be time dependent. Reaction occurred in a relatively fast way and 50% of Cys186 was covalently modified after 1 h when **11C** was incubated at equimolar

Fig. 5. Concentration-dependent covalent modification of target Cys186 by derivatives **9C** and **11C** upon 24 h incubation as determined by LC-MS analysis. Data are the mean of two independent experiments, each performed in triplicate.
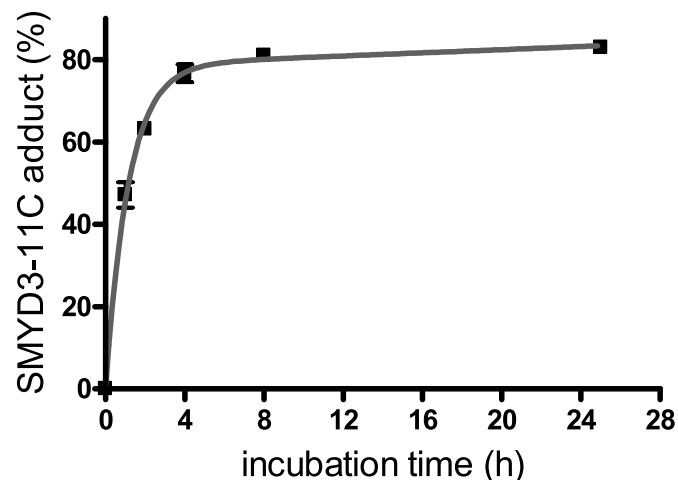

Fig. 6. Time course of the covalent adduct formation with Cys186 upon incubation of SMYD3 with **11C** at a molar ratio 1:1.

concentration with SMYD3 (Fig. 6).

2.5. Evaluation of inhibitory potency towards SMYD3 MTase activity and investigation of inhibition kinetics

The covalent modification of the cysteine residue in the substrate binding pocket is expected to translate into an enzyme activity inhibition, however covalent modification may not hamper substrate binding in an efficient way. To confirm the ability of the new derivatives to inhibit SMYD3 MTase activity, the inhibitory potency was assessed by a previously developed and validated MS-based approach [33] that does not require radio-ligands and ensures direct monitoring of methylated substrate formation. MAP3K2 peptide, representing the MAP3K2 sequence containing the SMYD3 target Lys260, was used as substrate. We tested all derivatives that showed any affinity in the SPR biosensor assay, since they can impair the substrate binding and inhibit SMYD3 MTase activity. Compounds were initially screened at a single concentration (10 μM, inhibitor/SMYD3 = 10), and the inhibitory activity of compounds bearing the Cys-trap, e.g., **9C** and **11C,** were compared to their analogs lacking the reactive group, i.e., **9** and **11**, respectively. EPZ031686 [25], as one of the most potent commercially available SMYD3 inhibitor, was used as a reference inhibitor, while **8C** was used as a negative control since it formed no reversible (SPR biosensor data) or covalent (MS data) adducts. Since different potencies were expected based on SPR biosensor and MS data, a relatively high inhibitor/target ratio (i.e., 10) was selected for a preliminary screening (Table 1).

Results in Table 1 show that **11C** and **9C** were significantly more potent than the corresponding reversible derivatives (**11C** *vs* **11** and **9C** *vs* **9**), confirming a role for the covalent adduct in the enzyme inhibition. Noticeably, data also proved that affinity plays a role (as expected for TCIs) since, in agreement with SPR biosensor results, also the reversible inhibitors with the affinity to SMYD3 in SPR biosensor screening, were able to inhibit MTase activity; the inhibitory potencies paralleled the affinity trend (see SPR biosensor studies). Indeed, the 5-cyclopropyloxy-azole fragment grants a higher affinity (**11** *vs* **9**; see SPR biosensor studies) which translated into a higher inhibitory potency.

11C showed the highest inhibition capacity among the new derivatives, close to that of the reference inhibitor EPZ031686. Also, when assayed at equimolar ratio with SMYD3, the inhibitory activity of **11C** ($51.7 \pm 0.7\%$) was comparable to that of EPZ031686 ($56.8 \pm 0.9\%$). However, due to the different mode of inhibition of **11C** compared to EPZ031686 (covalent *vs* reversible), we expected that a difference in the potency would appear upon a longer incubation time due to the time-dependent covalent bond formation. In agreement with this hypothesis, upon a 24 h-incubation compound **11C** inhibited SMYD3 MTase activity at a significantly higher extent with respect to EPZ031686 ($85.6 \pm 0.8\%$ *vs* $50.2 \pm 1.6\%$, respectively) when assayed at 1:1 ratio with SMYD3.

The kinetics of SMYD3 MTase activity inhibition by **11C** paralleled the kinetics of enzyme covalent modification at Cys186 (compare

profiles in Fig. S2 and Fig. 6). Indeed, formation of the covalent adduct impairs accessibility of the binding site to the substrate. IC_{50} value for compound **11C** upon 24 h incubation, i.e. a time which ensures covalent modification to reach the plateau (see Fig. S2), was calculated and resulted to be 370 ± 21 nM. In agreement with the above considerations, **11C** was more potent than the reference inhibitor EPZ031686 ($IC_{50} = 689 \pm 20$ nM) when assayed in the same experimental conditions [33]. Overall, these results indicated that **11C** has the most promising profile. Hence, this compound was selected for further investigations.

Finally, for an in-depth characterization of SMYD3 inhibition by **11C,** the kinetics of enzyme inactivation was also investigated. Indeed, inhibition by **11C** involves the initial formation of a reversible complex (EI), followed by production of a covalent adduct (EI*). Based on SPR biosensing studies, the formation of the covalent adduct EI* is much slower than the formation of the initial reversible complex EI, hence the two-step irreversible inhibitor model was applied [36]. In such an inactivation model, the inactivation constant K_I describes the affinity underpinning the initial non-covalent complex formation, while the maximum inactivation rate constant, k_{inact}, describes the rate of covalent adduct formation. For inhibition of SMYD3 by **11C**, K_I was 6.11 ± 0.11 μM, while k_{inact} resulted to be $(4.49 \pm 0.32) \, 10^{-4} \, s^{-1}$. From those values the inactivation potency, defined as k_{inact}/K_I, was calculated and resulted equals to $73.5 \, M^{-1}s^{-1}$.

2.6. Crystallographic analysis of 11C-SMYD3 complex

In order to confirm the mechanism of action of **11C**, the structure of SMYD3 in complex with **11C** was determined by X-ray crystallography. SMYD3 was conjugated with **11C** for 8 h at room temperature to allow the formation of a covalent bond with the target Cys186. The reaction mixture was subsequently used for crystallization trials. Optimal conditions revealed that acicular crystals nucleated within a day and grew to their maximal dimensions within one week. The crystals diffracted to a nominal resolution of 1.55 Å and belonged to $P2_12_12_1$ space group. Data collection, merging and scaling statistics are provided in Table S3 (Supplementary Information).

The model building involved the molecular replacement methods encompassing different refinement steps and placement of the co-crystallized substrate SAM. A continuous peak of positive difference electron density was observed at the bottom of the substrate protein binding cavity spanning a region between the entrance to the methylation tunnel and the target Cys186 (Fig. 7A). The structure shows that bound **11C** is located across one of SMYD3 β-strands formed by residues Phe183-Cys186. The opposite part of the inhibitor (represented by cyclopropyl-substituted oxazole group) is pointing towards SAM with the cyclopropyl substituent in close proximity to the entrance to the methylation tunnel formed by Phe183, Tyr239 and Tyr257.

Importantly, the data allowed the unambiguous assignment of all atoms in **11C,** with the only exception being the chlorine atom. No peak indicating its presence was observed. This result confirmed the reaction mechanism of **11C** towards Cys186 in which the chlorine of **11C** is a leaving group. Moreover, the distance between the sulphur atom of Cys186 and the continuous electron density between **11C** and the enzyme indicates the presence of a covalent bond between the protein and the inhibitor (Fig. 7B). The geometry of the thioether bond between Cys186 and α-carbon of the N-acetyl moiety of **11C** is optimal, with interatomic distances 1.8 Å and the C–S–C angle 107.5°.

In addition, the structure revealed one polar interaction between one carbonyl group of **11C** forming a hydrogen bond with the amide of Thr184. There were other polar contacts mediated through water molecules, namely, between the terminal carbonyl of **11C** and backbones of Ile214 and Phe216, as well as between the carbonyl of Cys238 and the aromatic nitrogen of the amide group. Finally, due to the high quality of the electron density map, we were able to assign a low energy chair conformation to the **11C** piperidine moiety.

Table 1
Inhibition of SMYD3 activity by compounds **9**, **9C**, **11** and **11C**. Molar ratio (inhibitor/SMYD3) = 10. EPZ031686 and **8C** were used as positive and negative controls, respectively. Data are the mean of two independent experiments each carried out in triplicate.

Compound	% inhibition[a] $\pm$ SD
EPZ031686	100.0 ± 0.0
11C	92.1 ± 0.4
11	29.1 ± 0.6
9C	14.0 ± 0.0
9	5.0 ± 0.7
8C	n.a.

[a] Preincubation time equals to 1 h. n.a stands for not active, i.e. inhibition percentage lower than 5%.
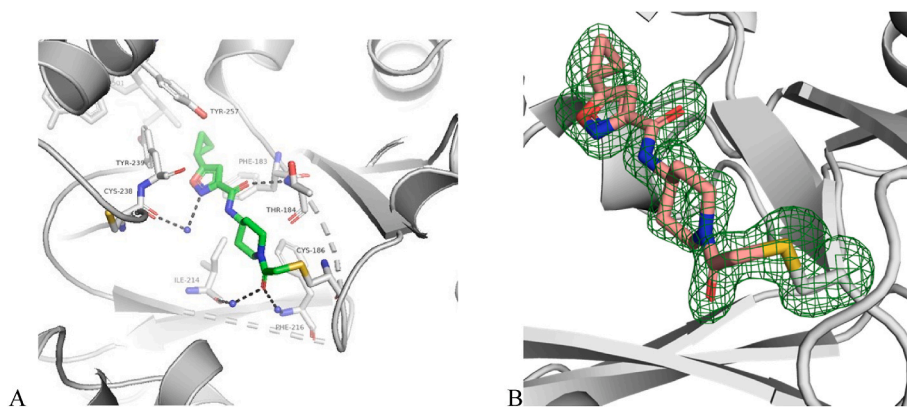
Fig. 7. X-Ray crystallographic structure of SMYD3 in complex with **11C**. A) The inhibitor is located at the bottom of the substrate binding site of SMYD3, spanning across the β-strand formed by amino acid residues 183–186 and establishing a covalent bond with Cys186. B) (F_0-F_c) difference density (green mesh), contoured at +3 sigma and carved at 1.6 Å from ***11C*** (salmon sticks) and side chain of Cys186 residue (grey sticks).

2.7. Plasma stability of 11C

The stability of compound **11C** in human plasma was evaluated by LC-MS analysis using propranolol as internal standard. No changes in **11C** concentration were observed within 3 h upon incubation at 37 °C. A 24% decrease was observed after a 6 h-incubation (Fig. 8).

2.8. Cell-based studies

As the best performing derivative in the series, the biological activity of compound **11C** was assessed in MDA-MB-231 breast cancer cells and HCT116 colorectal cancer cells. Compound **11**, the analog lacking the reactive warhead, was used as a reference. Two SMYD3 functions, namely epithelial-to-mesenchymal transition (EMT) [37] and regulation of RAS-ERK signalling [8,14], were specifically evaluated. MDA-MB-231 cells present mesenchymal-like features and a high invasiveness [38]. Based on preliminary dose-response experiments, we chose a 5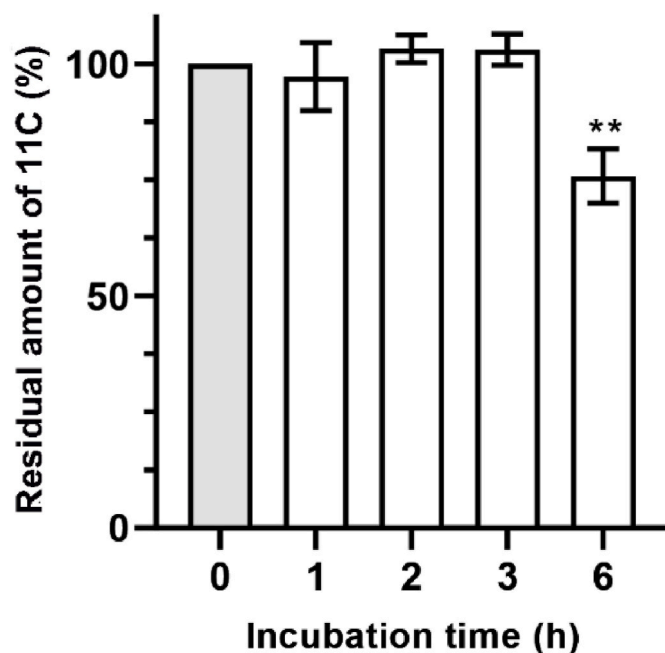 μM concentration as optimal dose to preliminarily study the impact of the **11** and **11C** on cell growth. In these cells **11C** significantly retarded cell proliferation by 48 h whereas **11** was without effect (Fig. 9).

Based on these results, we treated MDA-MB-231 cells with increasing concentrations of **11**, **11C** and EPZ031686 and investigated the steady-state levels of mRNAs of SMYD3 target genes by RT-qPCR. Specifically, **11C** was assayed at 0.5, 3.5 and 5 μM compared to 0.5, 5 and 50 μM for **11**. Similarly, higher doses were required for the reference compound EPZ031686 (10, 25 and 50 μM). Even at the lowest tested concentration (0.5 μM), **11C** significantly reduced the expression of *CDK2* and *C-MET*, the known SMYD3 regulated genes [14,20,39]. Furthermore, the abundance of mRNAs of the extracellular matrix component fibronectin 1 (FN1) and N-cadherin (N-CAD) [37] was attenuated by low micromolar concentrations of **11** (Fig. 10a). In contrast, the reversible analogue **11** was significantly less effective in affecting the expression of SMYD3 regulated genes (compare Fig. 10A and B). Furthermore, EPZ031686 evoked a lower efficacy, since the concentration as big as 50 μM and a longer exposure (72 h *vs* 48 h) were required to attenuate SMYD3 regulated transcripts (Fig. 10C). Conversely, the treatment with compound **11C** did not affect CDK2, C-MET, FN1 and N-CAD mRNA levels in SMYD3-KO-MDA-MB-231 cells, where the endogenous SMYD3 gene was knocked out by CRISPR/Cas9 genome editing (Fig. 10D) [31]. Likewise, compound **11C** did not alter transcript levels of the selected SMYD3 targets in a breast cancer cell line that expressed very low levels of SMYD3 and that we previously showed to be insensitive to the SMYD3 inhibitor BCI-121 (Fig. 10E) [14]. The finding that treatment with **11C** does not determine alterations in the transcript levels of

Fig. 8. Plasma stability of **11C**. The residual portion (%) of **11C** (10 μM input) over time at 37 °C in the plasma. Initial concentration of **11C** was set as 100%. Experiments were carried out in duplicate. (**) p = 0.020.
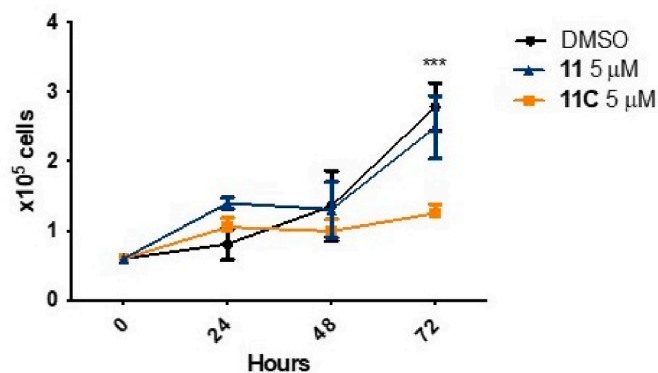

Fig. 9. Impact of compounds **11** and **11C** on MDA-MB-231 cell proliferation. DMSO (0.5%) was used as a vehicle. Statistical significance was calculated using a one-way ANOVA followed Tukey post-test. Data represents mean ± SD, n = 3.
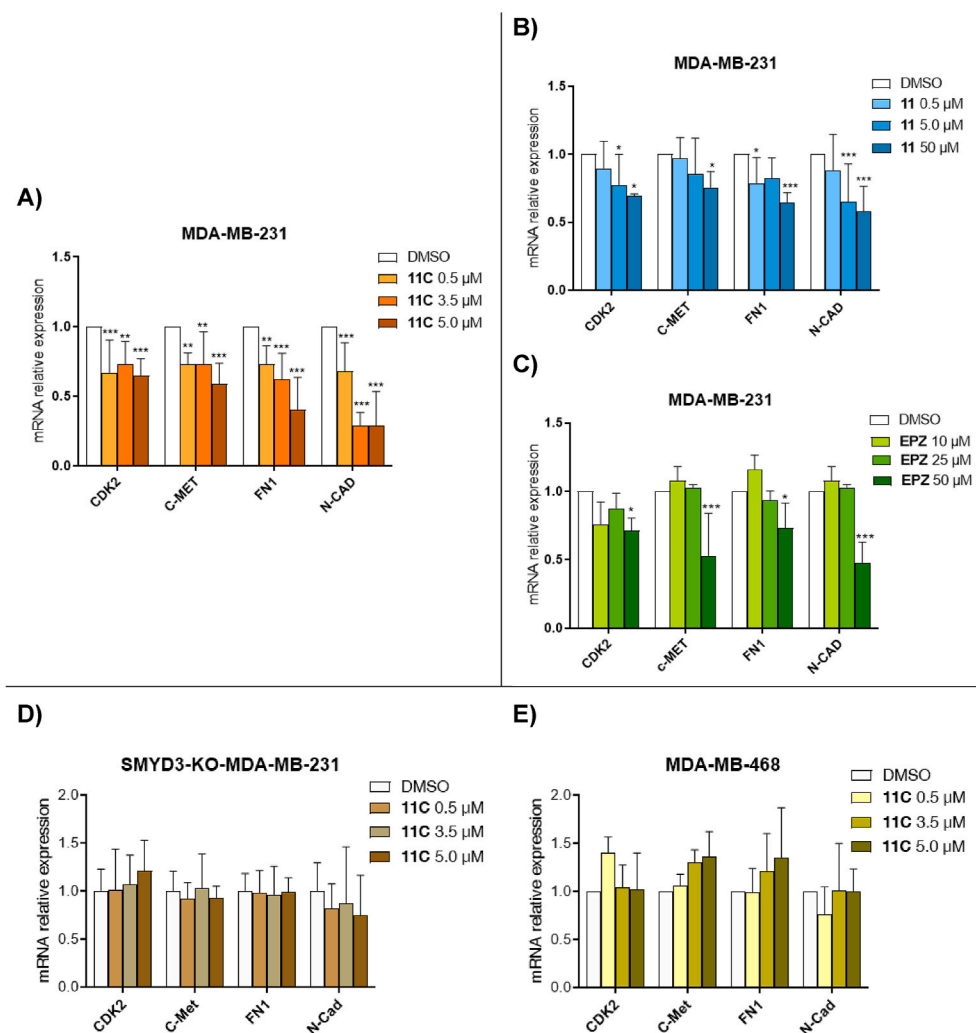
Fig. 10. Compound **11C** attenuates the expression of SMYD3 target genes while does not affect expression when SMYD3 is knocked out or expressed at low levels. qRT-PCR analysis of *CDK2*, c-*MET*, *FN1* and *N-CAD* transcripts in MDA-MB-231 cells treated with **11C** (A), **11** (B) (48 h) or for 72 h with EPZ031686 **(EPZ)** (C); qRT-PCR analysis of *CDK2*, c-*MET*, *FN1* and *N-CAD* transcripts in SMYD3-KO-MDA-MB-231 cells (D) and MDA-MB-468, a breast cancer cell line expressing low levels of SMYD3 (E) treated with **11C**. Data were normalized to the *GAPDH* housekeeping gene. Results were analysed with a two-way ANOVA followed by Dunnet post-test. *$p \leq 0.05$, **$p \leq 0.01$, ***$p \leq 0.001$. Data are mean $\pm$ SD; n $\geq$ 3.

SMYD3-regulated genes in cells where SMYD3 is very low or knocked out supports the idea that **11C** likely acts specifically through SMYD3.

SMYD3 has a pivotal role in the regulation of oncogenic RAS signalling by methylating MAP3K2 and modulating ERK1/2 phosphorylation/activation. SMYD3 deletion or pharmacological inhibition resulted in a lower ERK1/2 phosphorylation concomitant with reduced MEK-ERK signaling and *in vivo* tumour growth in response to oncogenic RAS [8,14]. Hence, the effect of SMYD3 inhibition was investigated using ERK1/2 phosphorylation as a readout in HCT116 and MDA-MB-231 cell lines that carry oncogenic *KRAS* mutations. Both compounds **11** and **11C** decreased ERK1/2 phosphorylation in a dose-

and time-dependent manner, with **11C** exerting a more potent effect in each cell line (Fig. 11). As RAS pathway inhibition induces growth inhibition and apoptosis of KRAS-mutant cells [40], PARP cleavage upon treatment with **11** and **11C** was also analysed. Fig. 11 showed that, in HCT116 as well as in MDA-MB-231 cells, **11C** attenuated ERK1/2 phosphorylation and induced PARP processing at the same concentrations that retarded cell proliferation (see Fig. 9). On the contrary, **11** did not induce these responses, in agreement with the lack of a significant inhibition of cell proliferation. Altogether, these results strongly suggested that, at least in certain cell types, cancer cell lines expressing high levels of SMYD3 are addicted to its enzymatic activity and appear to be
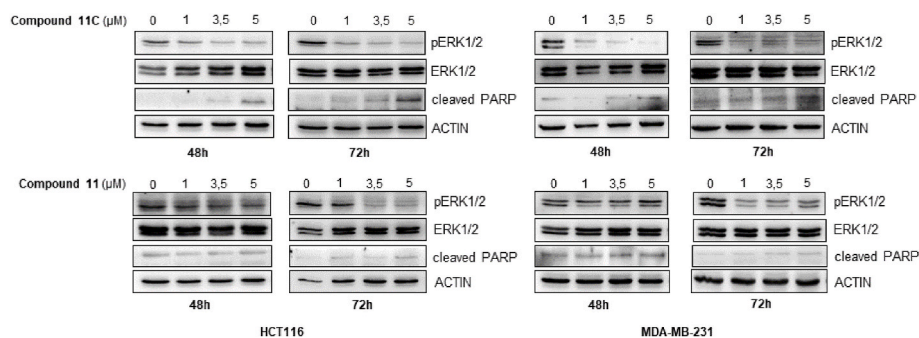

Fig. 11. Effects of compounds **11** or **11C** on ERK1/2 phosphorylation (pERK1/2) and PARP cleavage (cleaved PARP) in HCT116 and MDA-MB-231 cell lines analysed by immunoblotting. Actin was used as a loading control.

highly sensitive to its pharmacological inhibition with the covalent inhibitor **11C**.

3. Conclusions

We identified EM127 (**11C**) as the most perspective compound of a series of 4-aminopiperideine derivatives developed as targeted covalent inhibitors of SMYD3 methyltransferase. In line with the original design of SMYD3-directed TCIs, SPR biosensor experiments demonstrated that EM127 mode of action entails the formation of a reversible and stable complex (K_D value of 13.2 μM) with SMYD3 prior to covalent reaction. Formation of such a complex ensures the correct positioning of the inhibitor warhead within the enzyme binding pocket and grants the high selectivity for the target Cys186 residue, as evidenced by MS analyses and crystallographic data. Time dependent inhibition of SMYD3 MTase activity associated with a prolonged enzyme silencing is considered therapeutically beneficial. Data on knockout mice have shown that SMYD3 is dispensable for animal survival under physiological conditions, so pharmacological SMYD3 inhibition should be well tolerated.

EM127 effectively impaired the proliferation of MDA-MB-231 cells and reduced the transcriptional modulation of SMYD3 target genes. Moreover, EM127 affected ERK1/2 phosphorylation in HCT116 and MDA-MB-231 cell lines, suggesting that covalent inhibitors of SMYD3 can provide a long-lasting pharmacological action in specific tumor types expressing high levels of SMYD3.

Our results established EM127 as the first example of second-generation potent, selective, site-specific and covalent SMYD3 inhibitor. The newly discovered chemotype may serve as a chemical tool for further SMYD3 exploration. Development of drug candidates based on the new scaffold might be promising for treatment of SMYD3 positive tumors alone and in combination with PARP inhibitors.

4. Experimental section

Chemistry. *General procedures*. All reagents were used as obtained from commercial sources unless otherwise indicated. Solvents were dried over standard drying agents and freshly distilled prior to use. The ^{1}H and ^{13}C NMR spectra were recorded on Varian spectrometers (400 and 500 MHz for ^{1}H, 100 and 125 MHz for ^{13}C). Deuterated chloroform was used as the solvent for NMR experiments, unless otherwise stated. ^{1}H chemical shifts values (δ) are referenced to the residual non-deuterated components of the NMR solvents (δ = 7.26 ppm for CHCl$_3$). The ^{13}C chemical shifts (δ) are referenced to CDCl$_3$ (central peak, δ = 77.0 ppm), as the internal standard. Mass spectrometry analyses were performed by direct infusions on a Q-ToF Micro quadrupole time-of-flight (Q-TOF) hybrid analyzer (Micromass, Manchester, UK) equipped with a Z-spray electrospray ion source (ESI) operating in positive polarity. Flash chromatography was performed on Teledyne Isco CombiFlash® Rf 200 using RediSep® Normal-phase Silica Flash Columns (230–400 mesh). TLC was performed on silica gel 60 F254 plastic sheets. Purity of final compounds was determined on a Jasco HPLC system (model: Jasco PU-2089 equipped with MD-2010 DAD detector) under optimized chromatographic conditions (supporting information).

***tert*-butyl 4-(2-chloroacetamido)piperidine-1-carboxylate (2).** 2-chloro acetylchloride (0.45 mmol, 37 μL, 1.5 eq.) was added dropwise to a solution of *tert*-butyl 4-aminopiperidine-1-carboxylate (**1**) (0.3 mmol, 62 mg, 1 eq.) and pyridine (0.45 mmol, 36 μL, 1.5 eq.) in CH$_2$Cl$_2$ (3 mL) at 0 °C. The reaction mixture was then transferred into a separatory funnel and subsequently washed with a saturated solution of NH$_4$Cl and brine. The organic layer was dried over Na$_2$SO$_4$, filtered and concentrated under reduced pressure. The crude product was purified by silica gel column chromatography (*c*Hex:AcOEt 70:30) to give compound **2** as a white solid in 90% yield. ^{1}H NMR (500 MHz, CDCl$_3$) δ 6.45 (d, J = 7.7 Hz, 1H), 4.06–4.03 (m, 2H), 4.03 (s, 2H) 3.97-3.89 (m, 1H), 2.87 (ddd, J = 14.1, 11.5, 2.8 Hz, 2H), 1.93-1.89 (m, 2H), 1.45 (s, 9H),

1.41–1.32 (m, 2H). ^{13}C NMR (126 MHz, CDCl$_3$) δ 165.26, 154.51, 79.64, 47.14, 42.52 (2C), 42.47, 31.58 (2C), 28.33 (3C).

***tert*-butyl (1-(5-methylisoxazole-3-carbonyl)piperidin-4-yl) carbamate (6).** To a solution of 5-methylisoxazole-3-carboxylic acid (**4**, 0.2 mmol, 1 eq.), N-Boc-4-aminopiperidine (0.2 mmol, 40 mg, 1equiv.) and DMAP (0.24 mmol, 29 mg, 1.2 equiv.) in DCM (2mL), EDC (0.24 mmol, 46 mg, 1.2 equiv.) was added in one portion. The resulting mixture was stirred at room temperature overnight. Subsequently, the volatiles were removed under reduced pressure and the crude was purified by silica gel column chromatography (*c*Hex:AcOEt = 60:40) affording compound **6** as a white solid in 53% yield. ^{1}H NMR (500 MHz, CDCl$_3$) δ 6.25 (bs, 1H), 4.59 (d, J = 13.6 Hz, 1H), 4.51 (bs, 1H), 4.35 (dtd, J = 13.9, 3.9, 2.1 Hz, 1H), 3.75-3.71 (m, 1H), 3.22 (ddd, J = 14.3, 11.6, 2.7 Hz, 1H), 2.97–2.91 (m, 1H), 2.46 (s, 3H), 2.07–1.99 (m, 2H), 1.44 (s, 9H), 1.42-1.37 (m, 2H). ^{13}C NMR (126 MHz, CDCl$_3$) δ 169.93, 159.81, 158.65, 155.06, 102.68, 79.66, 47.82, 45.84, 41.48, 33.19, 32.16, 28.37 (3C), 12.14.

tert-butyl (1-(5-cyclopropylisoxazole-3-carbonyl)piperidin-4-yl)carbamate (7). Compound **7** was prepared starting form 5-cyclopropylisoxazole-3-carboxylic acid (**5**) and following the procedure described for the synthesis of derivative **6**. **7** was isolated as a white solid by silica gel column chromatography (*c*Hex:AcOEt 50:50) in 96% yield. ^{1}H NMR (500 MHz, CDCl$_3$) δ 6.16 (s, 1H), 4.59 (d, J = 13.2 Hz, 1H), 4.47 (bs, 1H), 4.37-4.33 (m, 1H), 3.75 (bs, 1H), 3.22 (ddd, J = 14.2, 11.7, 2.8 Hz, 1H), 2.98–2.92 (m, 1H), 2.10-2.01 (m, 3H), 1.46 (s, 9H), 1.43–1.36 (m, 2H), 1.14–1.08 (m, 2H), 1.03–0.97 (m, 2H). ^{13}C NMR (126 MHz, CDCl$_3$) δ 175.39, 159.81, 158.54, 155.07, 99.70, 79.62, 47.83, 45.82, 41.45, 33.15, 32.13, 28.36 (3C), 8.66, 8.65, 8.01.

(4-aminopiperidin-1-yl)(5-methylisoxazol-3-yl)methanone hydrochloride (8). 2.0 mL of HCl 2 M were added to a solution of compound **6** (0.19 mmol, 64.4 mg, 1 eq.) dissolved in MeOH (2.0 mL). The reaction mixture was stirred until complete conversion of the starting material (monitored by TLC). Volatiles were removed under reduced pressure affording pure compound **8** as a white solid in quantitative yield. ^{1}H NMR (400 MHz, D$_2$O) δ 6.21 (s, 1H), 4.47–4.43 (m, 1H), 3.90-3.86 (m, 1H), 3.39–3.88 (m, 1H), 3.13-3.10 (m, 1H), 2.89-2.83 (m, 1H), 2,32 (s, 3H), 2.03–1.91 (m, 2H), 1.53–1.47 (m, 2H). ^{13}CNMR (100 MHz, D$_2$O) δ 172.32, 161.80, 157.58, 152.93, 101.37, 101.30, 47.63, 45.39, 40.65, 29.68, 28.01, 11.27. Monoisotopic MS (ESI) m/z: [M+H]$^+$ calc for C$_{10}$H$_{15}$N$_3$O$_2$, 210.1242; found 210.1274; Anal. HPLC: Rt 10.60 min, purity 95.0%.

(4-aminopiperidin-1-yl)(5-cyclopropylisoxazol-3-yl)methanone hydrochloride (9). For the preparation of compound **9**, the same procedure used for **8** synthesis was applied. At the end of reaction, monitored by TLC, volatiles were removed under reduced pressure affording pure compound **9** as a white solid in quantitative yield. ^{1}H NMR (500 MHz, D$_2$O) δ 6.14 (s, 1H), 4.47–4.44 (m, 1H), 3.87 (d, J = 14.1 Hz, 1H), 3.44–3.38 (m, 1H), 3.13 (t, J = 13.3 Hz, 1H), 2.87 (t, J = 13.0 Hz, 1H), 2.07–1.93 (m, 2H), 1.95 (d, J = 12.8 Hz, 1H), 1.54–1.48 (m, 2H), 1.03–0.99 (m, 2H), 0.87–0.83 (m, 2H). ^{13}CNMR (100 MHz, D$_2$O) δ 177.66, 161.75, 157.58, 152.39, 98.09, 98.01, 47.64, 45.39, 40.63, 29.70, 28.81, 8.37, 7.41. Monoisotopic MS (ESI) m/z: [M+H]$^+$ calc for C$_{12}$H$_{17}$N$_3$O$_2$, 236.1399; found 236.1189; Anal. HPLC: Rt 6.87 min, purity 99.7%.

2-chloro-*N*-(1-(5-methylisoxazole-3-carbonyl)piperidin-4-yl) acetamide (8C). 2 mL of HCl 2 M were added to a solution of compound **2** (0.2 mmol, 55 mg) and MeOH (2 mL). The reaction mixture was stirred until complete conversion (monitored by TLC). Afterward, volatiles were removed under reduced pressure and the crude product (**3**) was used in the next step without further purification. 5-methylisoxazole-3-carboxylic acid (**4**, 0.2 mmol, 1 eq.), DIPEA (0.5 mmol, 87 μL, 2.5 eq.) and EDC (0.24 mmol, 46 mg, 1.2 eq.) were added in one portion to a solution of **3** in CH$_2$Cl$_2$ (2 mL). The resulting mixture was stirred at room temperature overnight. The volatiles were removed under reduced pressure and the crude was purified by silica gel column chromatography (*c*Hex:AcOEt 30:70), affording derivative **8C** as a white solid in

40% yield. **¹H NMR** (500 MHz, CDCl₃) δ 6.53 (d, J = 8.0 Hz, 1H), 6.26–6.25 (m, 1H), 4.68–4.63 (m, 1H), 4.43–4.39 (m, 1H), 4.09 (dddd, J = 15.6, 11.3, 8.4, 4.3 Hz, 1H), 4.04 (s, 2H), 3.24 (ddd, J = 14.2, 11.9, 2.8 Hz, 1H), 2.95 (ddd, J = 13.6, 12.0, 3.0 Hz, 1H), 2.46 (d, J = 1.0 Hz, 3H), 2.10–2.00 (m, 2H), 1.57–1.47 (m, 2H). **¹³C NMR** (126 MHz, CDCl₃) δ 170.05, 165.32, 159.82, 158.56, 102.68, 47.04, 45.75, 42.55, 41.41, 32.53, 31.50, 12.14. Monoisotopic MS (ESI) m/z: [M+H]⁺ calc for C₁₂H₁₆ClN₃O₃, 286.0958; found 286.1003; Anal. HPLC: Rt 8.27 min, purity 98.8%.

2-chloro-*N*-(1-(5-cyclopropylisoxazole-3-carbonyl)piperidin-4-yl)acetamide (9C). Compound **9C** was obtained starting from 5-cyclopropylisoxazole-3-carboxylic acid (**5**) and following the same procedure described for the synthesis of derivative **8C**. **9C** was isolated by silica gel column chromatography (*c*Hex:AcOEt 40:60) as a white solid in 75% yield. **¹H NMR** (500 MHz, CDCl₃) δ 6.50 (d, J = 7.4 Hz, 1H), 6.16 (s, 1H), 4.67–4.63 (m, 1H), 4.43–4.39 (m, 1H), 4.13–4.06 (m, 1H), 4.04 (s, 2H), 3.24 (ddd, J = 14.3, 11.9, 2.8 Hz, 1H), 2.95 (ddd, J = 13.6, 12.0, 3.0 Hz, 1H), 2.09–2.01 (m, 3H), 1.56–1.47 (m, 2H), 1.12–1.08 (m, 2H), 1.01–0.98 (m, 2H). **¹³C NMR** (126 MHz, CDCl₃) δ 175.53, 165.29, 159.84, 158.48, 99.73, 47.04, 45.75, 42.55, 41.41, 32.54, 31.52, 8.71, 8.69, 8.03. Monoisotopic MS (ESI) m/z: [M+H]⁺ calc for C₁₄H₁₈ClN₃O₃, 312.1115; found 312.1090; Anal. HPLC: Rt 6.25 min, purity 99.7%.

***tert*-butyl 4-(5-cyclopropylisoxazole-3-carboxamido)piperidine-1-carboxylate (10).** To a solution of 5-cyclopropylisoxazole-3-carboxylic acid (**5**) (0.2 mmol, 31 mg, 1 eq.), *tert*-butyl 4-aminopiperidine-1-carboxylate **1** (0.2 mmol, 40 mg, 1 eq.) and DMAP (0.24 mmol, 29 mg, 1.2 equiv.) in CH₂Cl₂ (2 mL), EDC (0.24 mmol, 46 mg, 1.2 eq.) was added in one portion. The resulting mixture was stirred at room temperature overnight. The volatiles were removed under reduced pressure and the crude was purified by silica gel column chromatography (*c*Hex: AcOEt = 70:30) affording compound **10** as a white solid in 58% yield. **¹H NMR** (500 MHz, CDCl₃) δ 6.64 (d, J = 8.1 Hz, 1H), 6.32 (s, 1H), 4.11–4.03 (m, 3H), 2.90 (ddd, J = 14.2, 11.7, 2.8 Hz, 2H), 2.07 (tt, J = 8.5, 5.0 Hz, 1H), 2.00–1.94 (m, 2H), 1.46 (s, 9H), 1.44–1.37 (m, 2H), 1.14–1.09 (m, 2H), 0.98 (dt, J = 7.2, 4.8 Hz, 2H). **¹³C NMR** (126 MHz, CDCl₃) δ 176.90, 158.62, 158.42, 154.67, 98.32, 79.75, 46.86 (2C), 42.57, 31.83 (2C), 28.41 (3C), 8.79 (2C), 8.12.

5-cyclopropyl-*N*-(piperidin-4-yl)isoxazole-3-carboxamide hydrochloride (11). Compound **10** (0.12 mmol, 39 mg, 1 eq.) was dissolved in MeOH (1.5 mL) and then 1.5 mL of HCl 2 M were added. The reaction mixture was stirred until complete conversion was obtained (monitored by TLC). The volatiles were removed under reduced pressure, and **11** was isolated without any further purification in quantitative yield. **¹H NMR** (500 MHz, D₂O) δ 6.23 (d, J = 1.2 Hz, 1H), 4.03–3.99 (m, 1H), 3.36 (d, J = 12.9 Hz, 2H), 3.01 (dd, J = 14.2, 11.2 Hz, 2H), 2.08–2.00 (m, 3H), 1.71 (dd, J = 18.5, 8.3 Hz, 2H), 0.96–1.00 (m, 2H), 0.85–0.82 (m, 2H). **¹³CNMR** (100 MHz, D₂O) δ 177.67, 161.76, 157.61, 154.48, 91.11, 98.03, 47.64, 45.40, 40.64, 29.74, 28.84, 8.37, 7.42. Monoisotopic MS (ESI) m/z: [M+H]⁺ calc for C₁₂H₁₇N₃O₂, 236.1399; found 236.1354; Anal. HPLC: Rt 7.31 min, purity 100.0%.

***N*-(1-(2-chloroacetyl)piperidin-4-yl)-5-cyclopropylisoxazole-3-carboxamide (11C).** 2-chloro acethylchloride (0.17 mmol, 14 µL, 1.5 eq.) was added dropwise to a solution of compound **11** (0.116 mmol, 1 eq.) and DIPEA (0.29 mmol, 50 µL, 2.5 eq.) in CH₂Cl₂ (1.5 mL) at 0 °C. The resulting mixture was stirred at room temperature for 16 h and then transferred into a separatory funnel and washed with a saturated solution of NH₄Cl and brine. The organic layer was dried over Na₂SO₄, filtered and concentrated under reduced pressure. The crude product was purified by silica gel column chromatography (cHex:AcOEt 60:40) to give the compound **11C** as white solid in 96% yield. **¹H NMR** (500 MHz, CDCl3) δ 6.70 (d, J = 8.0 Hz, 1H), 6.32 (s, 1H), 4.54–4.50 (m, 1H), 4.22–4.14 (m, 1H), 4.13–4.04 (m, 2H), 3.92–3.84 (m, 1H), 3.30–3.24 (m, 1H), 2.90–2.84 (m, 1H), 2.14 (d, J = 12.9 Hz, 1H), 2.10–2.04 (m, 2H), 1.62–1.45 (m, 2H), 1.14–1.10 (m, 2H), 1.00–0.96 (m, 2H). **¹³C NMR** (126 MHz, CDCl₃) δ 177.02, 165.04, 158.55, 158.45, 98.29, 46.51, 45.15, 41.18, 40.97, 32.22, 31.34, 8.82 (2C), 8.13. Monoisotopic MS

(ESI) m/z: [M+H]⁺ calc for C₁₄H₁₈ClN₃O₃, 312.1115; found 312.1090; Anal. HPLC: tR 6.99 min, purity 99.3%.

SMYD3 production and purification. Full length recombinant SMYD3 was overexpressed in *E. coli* Rosetta 2 (a derivative of BL21 (DE3)) strain as previously reported [33]. The homogeneity of the isolated protein exceeded 98%, with an average yield of 5 mg of the pure protein from 1 L of culture. The high purity of the protein preparations was confirmed by mass spectrometry (MS) analysis. For crystallization experiments, the protein was purified by immobilized metal affinity chromatography (IMAC), followed by tag cleavage with thrombin, reverse IMAC, and anion exchange chromatography. Fractions containing pure protein were concentrated to 12 mg mL⁻¹ in 50 mM Tris-HCl (pH 8.0), 150 mM NaCl, 2 mM DTT buffer.

Interaction kinetic analysis. Interaction kinetic analyses were performed employing a BIAcore X100 system thermostated at 15 °C. SMYD3 surfaces preparation, experiments execution and data analysis were performed according to the previously published protocol. Briefly, SMYD3 was immobilized at densities between 6500 and 10000 RUs through amine-coupling chemistry employing CM5 sensor chips. For the immobilization procedure, HEPES 10 mM, NaCl 150 mM and T-20 0.05% at pH 7.4 (HBS-T) was used as running buffer. Tris-HCl 50 mM, NaCl 150 mM, 2 mM DTT, 0.05% T-20, DMSO 2% pH 8.0 was used as analysis buffer (TBS-T buffer). EM-compounds stock solutions were prepared at 10 mM concentration in 100% DMSO and diluted to 200 µM in TBS-T buffer so that final DMSO content equals 2%. Interactions were monitored in TBS-T buffer and TBS-T buffer supplemented with SMYD3-saturating concentration of S-adenosyl-methionine (SAM). S-adenosyl-homocysteine (SAH) and peptide MAP3K2₂₄₉₋₂₇₄ (DYDNPI-FEKFGK₂₆0GGTYPRRYHVSYHH; Celtek Peptides, Franklin, USA) were used as control compounds in SAM-free and SAM-saturated running buffer, respectively. A solvent correction procedure was performed and applied to equilibrium responses for data analysis. Data analysis was performed using BIAeval 4.1 and GraphPad software.

Mass spectrometry analysis of covalent binding. SMYD3 stock solution was prepared in Tris 50 mM pH 8.0 containing NaCl 150 mM, DTT 2 mM and glycerol 5% (v/v) and was stored at −80 °C before use. **8C**, **9C** and **11C** 10 mM stock solutions were prepared in DMSO and stored at −20 °C before use. Further enzyme and tested compounds dilutions were performed with Tris 50 mM pH 8.0 buffer containing 75 mM NaCl. To assess the formation of covalent bonds between SMYD3 and tested compounds, the enzyme (final concentration 10 µM) was incubated at 23 °C (Thermomixer Comfort) in their absence and presence. **8C** and **9C** were tested at the final concentration 10 and 100 µM while **11C** was also tested at the final concentration 1 µM. Samples (40 µL) were then denatured, alkylated and digested as described below. The rate of covalent bond formation between SMYD3 and **11C** was derived incubating SMYD3 at 23 °C in the presence of **11C** under equimolar conditions (10 µM). The resulting solution was incubated at 23 °C (Thermomixer Comfort) and, at selected times (0, 1, 2, 4, 8 and 24 h), an aliquot (40 µL) was drawn from the solution and immediately denatured, alkylated and digested. Enzyme denaturation was achieved by adding 5 µL of DTT 0.1 M in water and incubating at 56 °C for 30 min. After that iodoacetamide (IAA) 55 mM in Tris 50 mM pH 8.0 buffer containing 75 mM NaCl was added, and samples were incubated for 45 min in the dark. Finally, 2 µL of trypsin 1 µg/µL and 2 µL of chymotrypsin 1 µg/µL both in HCl 2 mM were added and samples were overnight incubated at 30 °C (Thermomixer Comfort) under gentle stirring (300 rpm). The resulting peptides were analysed by liquid chromatography-mass spectrometry analysis.

Liquid chromatography-mass spectrometry analysis. Peptides derived from SMYD3 proteolytic digestion were analysed by using an Agilent 1200 Series system (Walbronn, Germany) equipped with an autosampler. Analyses were performed on a reverse phase C4 column (Phenomenex Jupiter; 150 × 2.0 mm i.d., 5 µm, 300 Å) kept at 40 °C. Mobile phases A (water/AcCN/FA, 99/1/0.1) and B (AcCN/water/FA, 99/1/0.1) were used to develop a gradient. The solvent gradient was set

as follows: 0–40% B, 60 min; 40–70% B, 5 min; 70–80%, 10 min. The column was equilibrated with the mobile phase composition of the starting conditions for 10 min before the next injection. The flow rate was 0.4 mL/min while the injection volume was 18 μL. MSMS analysis for the identification of the peptides involved in the covalent bound with tested compounds was performed on a Q-ToF Micro hybrid analyser (Micromass, Manchester, UK) equipped with a Z-spray ion source. ESI-Q-TOF source temperature was set at 110 °C, the capillary voltage at 3.0 kV, and the cone voltage at 35 V. Peptide ions within a m/z 200–3600 survey scan mass range were analysed for subsequent fragmentation. 1^+, 2^+, 3^+ and 4^+ charged ions exceeding a threshold abundance (TIC value: 10 counts/sec), were selected for MSMS analyses. From a single survey scan 8 ions were selected for subsequent fragmentation. Scan returned to mass survey mode when the ion intensity fell below 5 counts/sec or after 8 s. Scan time was 1 s for the parent ion and 1 s for the fragment ions. Collision energy was selected using charge state recognition. Once identified the SMYD3 peptides involved in the formation of covalent bonds with tested compounds, TIC detection in the m/z range 200–3600 was employed and the percentage of the bound peptide was derived by applying the following formula:

$$\%\text{covalent binding} = [I_{\text{bound peptide}}/(I_{\text{bound peptide}} + I_{\text{free peptide}})] \times 100$$

where $I_{\text{bound peptide}}$ and $I_{\text{free peptide}}$ are the peptide intensity, both in its bound and free form, derived from the respective extract ion chromatogram. The analyses were performed in triplicate. Data were processed using GraphPad Prism 8.1.1 software. Best fitting was achieved by using a two-phase exponential association equation.

MTase inhibition assay. SMYD3 stock solution in 50 mM Tris buffer pH 8.0 containing 150 mM NaCl, 2 mM DTT and 5% glycerol (v/v) was stored at −80 °C before use. MAP3K2$_{249-274}$ peptide tested compounds and 10 mM EPZ031686 stock solutions were prepared in DMSO and stored at −20 °C before use. SAM stock solution (37.7 mM) was prepared in water and stored at −20 °C before use. All further dilutions were performed in assay buffer (Tris 50 mM pH 8.0 containing, 4 mM MgCl$_2$, 0.2% (v/v) Tween 20, 2 mM DTT). MAP3K2$_{249-274}$ peptide dilutions were performed with the assay buffer containing 10% DMSO (v/v).

SMYD3 was pre-incubated in the absence or presence of tested compounds at 23 °C for 1 h (Thermomixer Eppendorf Comfort) so that SMYD3 final concentration was 5 μM, tested compound final concentration was 50 μM and DMSO was 2% (v/v). All the tested compounds were preincubated at the concentration 50 μM for 1 h while **11C** and EPZ031686 were also pre-incubated at the concentration of 5 μM for 1 and 24 h. The SMYD3 MTase activity was assayed by incubating 6 μL of preincubated solutions with 5 μL of 300 μM SAM, 5 μL of MAP3K2$_{249-274}$ peptide (75 μM) and 14 μL of the assay buffer. In the final conditions SMYD3 was 1 μM. After 1 h of incubation at 30 °C the MTase activity of SMYD3 was stopped adding 30 μL of stop solution consisting of H$_2$O/AcCN/FA (50/50/0.1, v/v/v) and 10 μL were analysed by LC-ESI-MS as reported below. All experiments were performed in duplicate.

Inhibition kinetics of SMYD3 MTase activity by 11C.

Initial assessment of time dependent SMYD3 inhibition by 11C. SMYD3 was pre-incubated in the absence and in the presence of **11C** at 23 °C (Thermomixer Eppendorf Comfort, Eppendorf Italy) in the assay buffer so that SMYD3 and **11C** concentration was 5 μM and DMSO was 2% (v/v). At selected times (0, 1, 2, 4, 8 and 24 h), an aliquot (6 μL) was drawn from the solution and its MTase activity was assessed as reported in section 1.2.2. Final assay concentrations were: SMYD3 1 μM, **11C** 1 μM, MAP3K2$_{249-274}$ peptide 12.5 μM, SAM 50 μM and the final percentage of DMSO 2% (v/v). 10 μL of the final solution were analysed by LC-ESI-MS as reported below. All experiments were performed in duplicate. Data were processed using GraphPad Prism 8.1.1 software.

Determination of k_{inact} and K_I values for SMYD3 inhibition by 11C. k_{inact} and K_I values were determined applying the preincubation time-dependent inhibition with dilution approach [36]. SMYD3 (5 μM) was pre-incubated in the absence and in the presence of increasing

concentrations of **11C** (3.13, 6.25, 12.0 and 25.0 μM) at 23 °C (Thermomixer Eppendorf Comfort, Eppendorf Italy) in the assay. DMSO was kept at 2% (v/v). At selected times (1.5, 3, 5, 8, 13 and 24 h), an aliquot (6 μL) was drawn from the solution and its MTase activity was assessed as reported in section 1.2.2. In selected experimental conditions the percentage of substrate conversion was about 10% in agreement with model requirements. Data were processed using GraphPad Prism 8.1.1 software (Graph Pad Prism). In details, from one phase exponential decay curves the concentration dependent k_{obs} were derived. k_{obs} values (s^{-1}) were then plotted against **11C** concentration [M] in the pre-incubation assay and fitted to the non linear template model included in the GraphPad Prism software and describing the equation: $k_{obs} = k_{inact}*$[I]/(K$_I$ + [I]). k_{inact} and K$_I$ were calculated from the k_{max} value and from the inhibitor concentration giving a k value equals to 1/2 k_{max}, respectively. Finally, the overall inactivation potency was calculated from the ratio k_{inact}/K$_I$ [36].

IC$_{50}$ determination. SMYD3 5 μM was pre-incubated in the absence or presence of **11C** at 23 °C for 24 h in the activity assay buffer. On the basis of its reversible mechanism of inhibition, the reference inhibitor EPZ031686 was pre-incubated with SMYD3 for 1 h. DMSO was 2% (v/v). MTase activity was determined as reported in section 1.2.2. Final assay concentrations were: SMYD3 1 μM, **11C** from 1.74 to 0.11 μM or EPZ031686 from 5 to 0.15 μM, MAP3K2$_{249-274}$ peptide 12.5 μM, SAM 50 μM and the final percentage of DMSO 2% (v/v). 10 μL of the final solution were analysed by LC-ESI-MS as reported below. All experiments were performed in duplicate. IC$_{50}$ was determined from the inhibition-concentration curves using GraphPad Prism (version 8.1.1).

LC-MS analysis. LC-MS analysis to assess the methylation degree on MAP3K2$_{249-274}$ peptide was carried out on Agilent 1200 HPLC instrument equipped with a thermostated autosampler and C4 reverse phase Jupiter 300 column (150✗2 mm i.d., 5 μm, 300 Å; Phenomenex, USA) kept at 60 °C, coupled to a Q-ToF mass-spectrometer with a Z-Spray ion source (Micromass, UK). Mobile phases A (H$_2$O/AcCN/FA, 99/1/0.1) and B (AcCN/H$_2$O/FA, 99/1/0.1) were used to develop a solvent gradient as follows: 10–60% B over 2 min and 60% B for 3 min. Mass-spectrometric detection was performed under the following setting: source temperature – 100 °C, desolvation temperature 250 °C, capillary voltage 3.0 kV, cone voltage 35V. Chromatograms were recorded in total ion current (TIC), in the m/z range 500–1700 and the scan time was 1 s. The peptide's baseline-subtracted spectra were deconvoluted onto a true mass scale using the maximum entropy (MaxEnt1)-based software supplied with MassLynx 4.1 software. LC-MS analyses were performed in duplicate.

Crystallization of SMYD3-11C complex. Compound **11C** (0.4 mM solubilized in DMSO) was incubated with SMYD3 (7 mg/ml in 50 mM Tris-HCl (pH 8.0), 150 mM NaCl, 2 mM DTT) at room temperature for 8 h. The crystallization was performed using hanging drop vapor diffusion method with 2 μL drops with equal volumes of reservoir solution (16% PEG3350, 100 mM Tris (pH 8.25), 100 mM Mg(OAc)$_2$) and SMYD3 incubated with compound **11C**. The crystals were cryocooled in liquid nitrogen after soaking in a cryoprotection solution containing 20% PEG3350, 100 mM Tris (pH 8.25), 100 mM Mg(OAc)$_2$, 10% DMSO and 10% glycerol. The data was collected at BioMAX beamline of MAX IV light source (Lund, Sweden). The structure was solved with molecular replacement employing PhaserMR software [41] and 5CCL as a search model, refinement was done with Refmac5 [42], model building with Coot [38], restrains for **11C** were quantified with ACEDRG [38]. Model quality was evaluated using MolProbity [43]. To obtain a (F$_0$-F$_c$) difference density map, ligand atoms and atoms SG, CB, CA of Cys186 residue were removed from the final model. Then, the map was calculated using Refmac5 after 10 cycles of refinement [44].

Determination of 11C stability in the plasma. A 5 μL aliquot of **11C** stock solution (210 μM in PBS buffer) was added to 100 μL of plasma from a healthy volunteer to reach the final inhibitor concentration of 10 μM. Samples were incubated at 37 °C, under gentle agitation (300 rpm, Thermomixer Comfort, Eppendorf). At selected time

(0, 60, 120, 180, and 360 min), plasma proteins were precipitated by addition of 400 μL of ice-cold acetonitrile containing propranolol as internal standard (IS, 625 nM). Each time point was assayed in triplicate. Samples were centrifuged at 13000 rcf for 10 min at 4 °C, then, 350 μL of supernatant were collected and dried under nitrogen stream. Finally, the residue was re-suspended in 100 μL of H_2O/AcCN (50/50, v/v) and analysed by a liquid chromatography-mass spectrometry (LC-MS) approach. LC analysis was carried out by an Agilent 1200 Series (Walbronn, Germany) equipped with an autosampler. Analyses were performed on a C18 (Eclipse XDB-C18, 3.5 μm; 2.1 × 100 mm; Agilent). A gradient elution was optimized with the mobile phase A [water/acetonitrile/formic acid (99/1/0.1) (v/v/v)] and B [acetonitrile/water/formic acid (99/1/0.1) (v/v/v)]. In particular B was increased from 15 to 50% in 8 min. The flow rate was set at 0.3 mL/min and the injection volume was 10 μL. Mass spectrometry analyses were performed on a Q-ToF spectrometer (Micromass, Manchester, UK) equipped with a Z-spray ion source. The ESI source temperature was set at 120 °C, the desolvation temperature at 280 °C, the capillary voltage at 3.0 kV, and the cone voltage at 35 V. Single ion monitoring (SIM) acquisitions in positive polarity were performed at 312 and 260 m/z for **11C** and IS, respectively. The ratio between **11C** and IS peak area was plotted against time to evaluate **11C** stability in plasma.

Cell based studies. HCT116, MDA-MB-231 and MDA-MB-468 cell lines were purchased from ATCC and cultured in Dulbecco modified Eagle's medium supplemented with glucose, 10% foetal bovine serum (#0270-106, Gibco) and 100 U/ml penicillin and 100 μg/ml streptomycin (#15140-122, Gibco) at 37 °C, 5% CO_2. SMYD3-KO-MDA-MB-231 cells were previously described in Sanese et al. [31].Cell lines were routinely tested for *Mycoplasma* contamination (#11–7048; Minerva Biolabs) and found negative throughout the study. Trypan blue was from Sigma Aldrich. Cells were treated with different doses of compound **11,** compound **11C,** and EPZ031686 (Medchem Express) and analysed at different time points. Cells treated with DMSO were used as a control.

Quantification of cell viability was assessed by trypan blue method and cell death of the reported cell lines were scored by counting. Supernatants (containing dead/floating cells) were collected, and the remaining adherent cells were detached by Trypsin/EDTA (Sigma). Cell pellets were resuspended in 1X PBS and 10 μL were mixed with an equal volume of 0.01% trypan blue solution. Viable cells (unstained, trypan blue negative cells) and dead cells (stained, trypan blue positive cells) were counted with a phase-contrast microscope. The percentages of viable and dead cells were calculated. The data shown in the results section are representative of three or more independent sets of experiments.

RNA isolation, cDNA preparation and qPCR analysis. Total RNA was extracted using TRI reagent (Sigma) according to the manufacturer's instruction. cDNA was synthesized on the RNA template (1 μg) using the High Capacity cDNA Reverse Transcription Kit (Applied Biosystem). qRT-PCR was performed in triplicate using 2X Xtra Master Mix (GeneSpin) on a CFX Connect Real-Time PCR Detection System (Bio-Rad). The qRT-PCR reactions were normalized to GAPDH as housekeeping gene. Relative quantification was done using the ddCT method. Primers used in this study can be found in Fenizia et al. [37].

Immunoblotting. Whole cell extracts were homogenized in the lysis buffer (50 mM Tris-HCl pH 7.4, 5 mM EDTA, 250 mM NaCl and 1% Triton X-100) supplemented with protease and phosphatase inhibitors (Roche). Twenty micrograms of protein extracts from each sample were denatured in the Laemmli buffer and loaded into a 7.5% SDS–polyacrylamide gel. Proteins were resolved electrophoretically, transferred onto a nitrocellulose membrane and probed with primary antibodies to ACTIN (#3700, Cell Signaling), cleaved PARP (G7341, Promega), phospho-ERK1/2 (Thr202/Tyr204) (#9106, Cell Signaling) or total ERK1/2 (#9102, Cell Signaling). Rabbit and mouse IgG conjugated with horseradish peroxidase (#NA934V and #NA931V, respectively; GE Healthcare) were used as secondary antibodies. Signals were detected using the ECL-plus chemiluminescence reagent (RPN2232, GE Healthcare).

Statistical analysis. Statistical significance of the results was analysed using Student's *t*-tail test. Differences p < 0.05 was considered statistically significant. You mentioned ANOVA and Tukey above.

PDB ID codes

6ZRB. Authors will release the atomic coordinates and experimental data upon article publication.

Author contributions

M.D.Parenti and M. Naldi contributed equally to this work.

Declaration of competing interest

The authors declare that they have no known competing financial interests or personal relationships that could have appeared to influence the work reported in this paper.

Data availability

No data was used for the research described in the article.

Acknowledgment

Appendix A. Supplementary data

Supplementary data to this article can be found online at https://doi.org/10.1016/j.ejmech.2022.114683.

References

[1] Y. Cheng, C. He, M. Wang, X. Ma, F. Mo, S. Yang, J. Han, X. Wei, Targeting epigenetic regulators for cancer therapy: mechanisms and advances in clinical trials, Signal Transduct. Targeted Ther. 4 (1) (2019), https://doi.org/10.1038/s41392-019-0095-0.

[2] B.J. Bernard, N. Nigam, K. Burkitt, V. Saloura, SMYD3: a regulator of epigenetic and signaling pathways in cancer, Clin. Epigenet. 13 (1) (2021) 1–19, https://doi.org/10.1186/s13148-021-01021-9.

[3] F. Andreoli, A. Del Rio, Physicochemical modifications of histones and their impact on epigenomics, Drug Discov. Today 19 (9) (2014) 1372–1379, https://doi.org/10.1016/j.drudis.2014.05.005.

[4] A. Del Rio, G. Varchi, Molecular design of compounds targeting histone methyltransferases, in: Epi-Informatics, 1st Edition Discovery and Development of Small Molecule Epigenetic Drugs and Probes, Academic press Elsevier, Amsterdam, 2016, pp. 257–272, https://doi.org/10.1016/B978-0-12-802808-7.00009-5.

[5] Y. Yoshioka, T. Suzuki, Y. Matsuo, G. Tsurita, T. Watanabe, N. Dohmae, Y. Nakamura, R. Hamamoto, Protein lysine methyltransferase SMYD3 is involved in tumorigenesis through regulation of HER2 homodimerization, Cancer Med. 6 (7) (2017) 1665–1672, https://doi.org/10.1002/cam4.1099.

[6] Y. Yoshioka, T. Suzuki, Y. Matsuo, M. Nakakido, G. Tsurita, C. Simone, T. Watanabe, N. Dohmae, Y. Nakamura, R. Hamamoto, SMYD3-Mediated lysine methylation in the PH domain is critical for activation of AKT1, Oncotarget 7 (46) (2016) 75023–75037, https://doi.org/10.18632/oncotarget.11898.

[7] Y. Yoshioka, T. Suzuki, Y. Matsuo, G. Tsurita, T. Watanabe, N. Dohmae, Y. Nakamura, R. Hamamoto, Protein lysine methyltransferase SMYD3 is involved in tumorigenesis through regulation of HER2 homodimerization, Cancer Med. 6 (7) (2017) 1665–1672, https://doi.org/10.1002/cam4.1099.

[8] P.K. Mazur, N. Reynoird, P. Khatri, P.W.T.C. Jansen, A.W. Wilkinson, S. Liu, O. Barbash, G.S. Van Aller, M. Huddleston, D. Dhanak, P.J. Tummino, R.G. Kruger, B.A. Garcia, A.J. Butte, M. Vermeulen, J. Sage, O. Gozani, SMYD3 links lysine methylation of MAP3K2 to Ras-driven cancer, Nature 510 (7504) (2014) 283–287, https://doi.org/10.1038/nature13320.

[9] A.M. Cock Rada, S. Medjkane, N. Janski, N. Yousfi, M. Perichon, M. Chaussepied, J. Chluba, G. Langsley, J.B. Weitzman, SMYD3 promotes cancer invasion by epigenetic upregulation of the metalloproteinase MMP-9, Cancer Res. 72 (3) (2012) 810–820, https://doi.org/10.1158/0008-5472.CAN-11-1052.

[10] L. Huang, A.-M. Xu, SET and MYND domain containing protein 3 in cancer, Am. J. Transl. Res. 9 (1) (2017) 1–14.

[11] S.-J. Ma, Y.-M. Liu, Y.-L. Zhang, M.-W. Chen, W. Cao, Correlations of EZH2 and SMYD3 gene polymorphisms with breast cancer susceptibility and prognosis, Biosci. Rep. 38 (1) (2018), https://doi.org/10.1042/BSR20170656.

[12] X.-G. Luo, C.-L. Zhang, W.-W. Zhao, Z.-P. Liu, L. Liu, A. Mu, S. Guo, N. Wang, H. Zhou, T.-C. Zhang, Histone methyltransferase SMYD3 promotes MRTF-A-mediated transactivation of MYL9 and migration of MCF-7 breast cancer cells, Cancer Lett. 344 (1) (2014) 129–137, https://doi.org/10.1016/j.canlet.2013.10.026.

[13] R. Hamamoto, F.P. Silva, M. Tsuge, T. Nishidate, T. Katagiri, Y. Nakamura, Y. Furukawa, Enhanced SMYD3 expression is essential for the growth of breast cancer cells, Cancer Sci. 97 (2) (2006) 113–118, https://doi.org/10.1111/j.1349-7006.2006.00146.x.

[14] A. Peserico, A. Germani, P. Sanese, A.J.A.J. Barbosa, V. di Virgilio, R. Fittipaldi, E. Fabini, C. Bertucci, G. Varchi, M.P.M.P. Moyer, G. Caretti, A. del Rio, C. Simone, A SMYD3 small-molecule inhibitor impairing cancer cell growth, J. Cell. Physiol. 230 (10) (2015) 2447–2460, https://doi.org/10.1002/jcp.24975.

[15] R. Hamamoto, Y. Furukawa, M. Morita, Y. Iimura, F.P. Silva, M. Li, R. Yagyu, Y. Nakamura, SMYD3 encodes a histone methyltransferase involved in the proliferation of cancer cells, Nat. Cell Biol. 6 (8) (2004) 731–740, https://doi.org/10.1038/ncb1151.

[16] F.Q. Vieira, P. Costa-Pinheiro, D. Almeida-Rios, I. Graça, S. Monteiro-Reis, S. Simões-Sousa, I. Carneiro, E.J. Sousa, M.I. Godinho, F. Baltazar, R. Henrique, C. Jerónimo, SMYD3 contributes to a more aggressive phenotype of prostate cancer and targets cyclin D2 through H4K20me3, Oncotarget 6 (15) (2015) 13644–13657, https://doi.org/10.18632/oncotarget.3767.

[17] C. Liu, C. Wang, K. Wang, L. Liu, Q. Shen, K. Yan, X. Sun, J. Chen, J. Liu, H. Ren, H. Liu, Z. Xu, S. Hu, D. Xu, Y. Fan, SMYD3 as an oncogenic driver in prostate cancer by stimulation of androgen receptor transcription, J. Natl. Cancer Inst. 105 (22) (2013) 1719–1728, https://doi.org/10.1093/jnci/djt304.

[18] J. Li, L. Zhao, Y. Pan, X. Ma, L. Liu, W. Wang, W. You, SMYD3 overexpression indicates poor prognosis and promotes cell proliferation, migration and invasion in non-small cell lung cancer, Int. J. Oncol. 57 (3) (2020) 756–766, https://doi.org/10.3892/ijo.2020.5095.

[19] X. Fei, Y. Ma, X. Liu, Z. Meng, Overexpression of SMYD3 is predictive of unfavorable prognosis in hepatocellular carcinoma, Tohoku J. Exp. Med. 243 (3) (2017) 219–226, https://doi.org/10.1620/tjem.243.219.

[20] C. Bottino, A. Peserico, C. Simone, G. Caretti, SMYD3: an oncogenic driver targeting epigenetic regulation and signaling pathways, Cancers (Basel) 12 (1) (2020) 1–18, https://doi.org/10.3390/cancers12010142.

[21] M.E. Sarris, P. Moulos, A. Haroniti, A. Giakountis, I. Talianidis, Smyd3 is a transcriptional potentiator of multiple cancer-promoting genes and required for liver and colon cancer development, Cancer Cell 1–13 (2016), https://doi.org/10.1016/j.ccell.2016.01.013.

[22] C. Huang, S.S. Liew, G.R. Lin, A. Poulsen, M.J.Y. Ang, B.C.S. Chia, S.Y. Chew, Z. P. Kwek, J.L.K. Wee, E.H. Ong, P. Retna, N. Baburajendran, R. Li, W. Yu, K. Koh-Stenta, A. Ngo, S. Manesh, J. Fulwood, Z. Ke, H.H. Chung, S. Sepramaniam, X. H. Chew, N. Dinie, M.A. Lee, Y.S. Chew, C.B. Low, V. Pendharkar, V. Manoharan, S. Vuddagiri, K. Sangthongpitag, J. Joy, A. Matter, J. Hill, T.H. Keller, K. Foo, Discovery of irreversible inhibitors targeting histone methyltransferase, SMYD3, ACS Med. Chem. Lett. (2019), https://doi.org/10.1021/acsmedchemlett.9b00170 acsmedchemlett.9b00170.

[23] E. Fabini, E. Manoni, C. Ferroni, A.D.A.D. Rio, M. Bartolini, Small-molecule inhibitors of lysine methyltransferases SMYD2 and SMYD3: current trends, Future Med. Chem. 11 (8) (2019) 901–921, https://doi.org/10.4155/fmc-2018-0380.

[24] D.S. Su, J. Qu, M. Schulz, C.W. Blackledge, H. Yu, J. Zeng, J. Burgess, A. Reif, M. Stern, R. Nagarajan, M.B. Pappalardi, K. Wong, A.P. Graves, W. Bonnette, L. Wang, P. Elkins, B. Knapp-Reed, J.D. Carson, C. McHugh, H. Mohammad, R. Kruger, J. Luengo, D.A. Heerding, C.L. Creasy, Discovery of isoxazole amides as potent and selective SMYD3 inhibitors, ACS Med. Chem. Lett. 11 (2) (2020) 133–140, https://doi.org/10.1021/acsmedchemlett.9b00493.

[25] L.H. Mitchell, P.A. Boriack-Sjodin, S. Smith, M. Thomenius, N. Rioux, M. Munchhof, J.E. Mills, C. Klaus, J. Totman, T.V. Riera, A. Raimondi, S.L. Jacques, K. West, M. Foley, N.J. Waters, K.W. Kuntz, T.J. Wigle, M.P. Scott, R.a. Copeland, J. J. Smith, R. Chesworth, Novel oxindole sulfonamides and sulfamides: EPZ031686, the first orally bioavailable small molecule SMYD3 inhibitor, ACS Med. Chem. Lett. 7 (2) (2016) 134–138, https://doi.org/10.1021/acsmedchemlett.5b00272.

[26] S. Gradl, H. Steuber, J. Weiske, M.M. Szewczyk, N. Schmees, S. Siegel, D. Stoeckigt, C.D. Christ, F. Li, S. Organ, M. Abbey, S. Kennedy, I. Chau, V. Trush, D. Barsyte-Lovejoy, P.J. Brown, M. Vedadi, C. Arrowsmith, M. Husemann, V. Badock, M. Bauser, A. Haegebarth, I.v. Hartung, C. Stresemann, Discovery of the SMYD3 inhibitor BAY-6035 using thermal shift assay (TSA)-Based high-throughput screening, SLAS Discovery 26 (8) (2021) 947–960, https://doi.org/10.1177/24725552211019409.

[27] M.J. Thomenius, J. Totman, D. Harvey, L.H. Mitchell, T.V. Riera, K. Cosmopoulos, A.R. Grassian, C. Klaus, M. Foley, E.A. Admirand, H. Jahic, C. Majer, T. Wigle, S. L. Jacques, J. Gureasko, D. Brach, T. Lingaraj, K. West, S. Smith, N. Rioux, N. J. Waters, C. Tang, A. Raimondi, M. Munchhof, J.E. Mills, S. Ribich, M. Porter Scott, K.W. Kuntz, W.P. Janzen, M. Moyer, J.J. Smith, R. Chesworth, R. A. Copeland, P.A. Boriack-Sjodin, Small molecule inhibitors and CRISPR/Cas9 mutagenesis demonstrate that SMYD2 and SMYD3 activity are dispensable for autonomous cancer cell proliferation, PLoS One 13 (6) (2018), e0197372, https://doi.org/10.1371/journal.pone.0197372.

[28] Y. Jiang, T. Lyu, X. Che, N. Jia, Q. Li, W. Feng, Overexpression of SMYD3 in ovarian cancer is associated with ovarian cancer proliferation and apoptosis via methylating H3K4 and H4K20, J. Cancer 10 (17) (2019) 4072–4084, https://doi.org/10.7150/jca.29861.

[29] F. Lin, D. Wu, D. Fang, Y. Chen, H. Zhou, C. Ou, STAT3-Induced SMYD3 transcription enhances chronic lymphocytic leukemia cell growth in vitro and in vivo, Inflamm. Res. 68 (9) (2019) 739–749, https://doi.org/10.1007/s00011-019-01257-5.

[30] C. Fasano, M. Lepore Signorile, K. de Marco, G. Forte, P. Sanese, V. Grossi, C. Simone, Identifying novel SMYD3 interactors on the trail of cancer hallmarks, Comput. Struct. Biotechnol. J. (2022), https://doi.org/10.1016/j.csbj.2022.03.037.

[31] P. Sanese, C. Fasano, G. Buscemi, C. Bottino, S. Corbetta, E. Fabini, V. Silvestri, V. Valentini, V. Disciglio, G. Forte, M. Lepore Signorile, K. de Marco, S. Bertora, V. Grossi, U. Guven, N. Porta, V. di Maio, E. Manoni, G. Giannelli, M. Bartolini, A. del Rio, G. Caretti, L. Ottini, C. Simone, Targeting SMYD3 to sensitize homologous recombination-proficient tumors to PARP-mediated synthetic lethality, iScience 23 (10) (2020), 101604, https://doi.org/10.1016/j.isci.2020.101604.

[32] V.O. Talibov, E. Fabini, E.A. FitzGerald, D. Tedesco, D. Cederfeldt, M.J. Talu, M. M. Rachman, F. Mihalic, E. Manoni, M. Naldi, P. Sanese, G. Forte, M. Lepore Signorile, X. Barril, C. Simone, M. Bartolini, D. Dobritzsch, A. Del Rio, U. H. Danielson, Discovery of an allosteric ligand binding site in SMYD3 lysine methyltransferase, Chembiochem 22 (9) (2021) 1597–1608, https://doi.org/10.1002/cbic.202000736.

[33] E. Fabini, V.O.V.O. Talibov, F. Mihalic, M. Naldi, M. Bartolini, C. Bertucci, A. Del Rio, U.H.H. Danielson, Unveiling the biochemistry of the epigenetic regulator SMYD3, Biochemistry 58 (35) (2019) 3634–3645, https://doi.org/10.1021/acs.biochem.9b00420.

[34] J. Singh, R.C. Petter, T. a Baillie, A. Whitty, The resurgence of covalent drugs, Nat. Rev. Drug Discov. 10 (4) (2011) 307–317, https://doi.org/10.1038/nrd3410.

[35] J.M. Bradshaw, J.M. McFarland, V.O. Paavilainen, A. Bisconte, D. Tam, V.T. Phan, S. Romanov, D. Finkle, J. Shu, V. Patel, T. Ton, X. Li, D.G. Loughhead, P.A. Nunn, D.E. Karr, M.E. Gerritsen, J.O. Funk, T.D. Owens, E. Verner, K.A. Brameld, R.J. Hill, D.M. Goldstein, J. Taunton, Prolonged and tunable residence time using reversible covalent kinase inhibitors, Nat. Chem. Biol. 11 (7) (2015) 525–531, https://doi.org/10.1038/nchembio.1817.

[36] E. Mons, S. Roet, R.Q. Kim, M.P.C. Mulder, A comprehensive guide for assessing covalent inhibition in enzymatic assays illustrated with kinetic simulations, Current Protocols 2 (6) (2022), https://doi.org/10.1002/cpz1.419.

[37] C. Fenizia, C. Bottino, S. Corbetta, R. Fittipaldi, P. Floris, G. Gaudenzi, S. Carra, F. Cotelli, G. Vitale, G. Caretti, SMYD3 promotes the epithelial-mesenchymal transition in breast cancer, Nucleic Acids Res. 47 (3) (2019) 1278–1293, https://doi.org/10.1093/nar/gky1221.

[38] P. Emsley, B. Lohkamp, W.G. Scott, K. Cowtan, Features and development of Coot, Acta Crystallogr. Sect. D Biol. Crystallogr. 66 (4) (2010) 486–501, https://doi.org/10.1107/S0907444910007493.

[39] V. Proserpio, R. Fittipaldi, J.G. Ryall, V. Sartorelli, G. Caretti, The methyltransferase SMYD3 mediates the recruitment of transcriptional cofactors at the myostatin and C-met genes and regulates skeletal muscle atrophy, Genes Dev. 27 (11) (2013) 1299–1312, https://doi.org/10.1101/gad.217240.113.

[40] P. Jasinski, P. Zwolak, K. Terai, A.Z. Dudek, Novel ras pathway inhibitor induces apoptosis and growth inhibition of K-Ras-Mutated cancer cells in vitro and in vivo, Transl. Res. 152 (5) (2008) 203–212, https://doi.org/10.1016/j.trsl.2008.09.001.

[41] A.J. McCoy, R.W. Grosse-Kunstleve, P.D. Adams, M.D. Winn, L.C. Storoni, R. J. Read, Phaser crystallographic software, J. Appl. Crystallogr. 40 (4) (2007) 658–674, https://doi.org/10.1107/S0021889807021206.

[42] G.N. Murshudov, P. Skubák, A.A. Lebedev, N.S. Pannu, R.A. Steiner, R.A. Nicholls, M.D. Winn, F. Long, A.A. Vagin, REFMAC 5 for the refinement of macromolecular crystal structures, Acta Crystallogr. Sect. D Biol. Crystallogr. 67 (4) (2011) 355–367, https://doi.org/10.1107/S0907444911001314.

[43] V.B. Chen, W.B. Arendall, J.J. Headd, D.A. Keedy, R.M. Immormino, G.J. Kapral, L. W. Murray, J.S. Richardson, D.C. Richardson, MolProbity : all-atom structure validation for macromolecular crystallography, Acta Crystallogr. Sect. D Biol. Crystallogr. 66 (1) (2010) 12–21, https://doi.org/10.1107/S0907444909042073.

[44] D. Liebschner, P.v. Afonine, M.L. Baker, G. Bunkóczi, V.B. Chen, T.I. Croll, B. Hintze, L.-W. Hung, S. Jain, A.J. McCoy, N.W. Moriarty, R.D. Oeffner, B.K. Poon, M.G. Prisant, R.J. Read, J.S. Richardson, D.C. Richardson, M.D. Sammito, O. v. Sobolev, D.H. Stockwell, T.C. Terwilliger, A.G. Urzhumtsev, L.L. Videau, C. J. Williams, P.D. Adams, Macromolecular structure determination using X-rays, neutrons and electrons: recent developments in phenix, Acta Crystallogr. Sec. D Struct. Biol. 75 (10) (2019) 861–877, https://doi.org/10.1107/S2059798319011471.